ELSEVIER

Journal of Quantitative Spectroscopy & Radiative Transfer 107 (2007) 263–293

Journal of Quantitative Spectroscopy & Radiative Transfer

www.elsevier.com/locate/jqsrt

A fast linearized pseudo-spherical two orders of scattering model to account for polarization in vertically inhomogeneous scattering–absorbing media

Vijay Natraj[a,*], Robert J.D. Spurr[b]

[a]*MC 150-21, Division of Geological and Planetary Sciences, California Institute of Technology, Pasadena, CA 91125, USA*
[b]*RT Solutions Inc., 9 Channing St., Cambridge, MA 02138, USA*

Received 18 October 2006; received in revised form 13 February 2007; accepted 14 February 2007

Abstract

We calculate the reflection matrix for the first two orders of scattering in a vertically inhomogeneous, scattering–absorbing medium. We take full account of polarization and perform a complete linearization (analytic differentiation) of the reflection matrix with respect to both the inherent optical properties of the medium and the surface reflection condition. Further, we compute a scalar–vector correction to the total intensity due to the effect of polarization; this correction is also fully linearized. The solar beam attenuation has been computed for a pseudo-spherical atmosphere.

Results from the two orders of scattering (2OS) model have been tested against scalar intensities for an inhomogeneous atmosphere, and against Stokes vector results for a homogeneous atmosphere. We have also performed backscatter simulations of reflected sunlight in the O_2 *A* band for a variety of geometries, and compared our results with those from a full vector multiple scattering code. Our results are exact in the center of strong lines and most inaccurate in the continuum, where polarization is least significant. The *s*- and *p*-polarized radiances are always computed very accurately. The effect of gas absorption optical depth, solar zenith angle, viewing geometry, surface albedo and wind speed (in the case of ocean glint) on the intensity, polarization and corresponding weighting functions have been investigated. It is shown that the 2OS model provides fast and reliably accurate polarization corrections to the scalar-model radiance and weighting function fields. The model can be implemented in operational retrieval algorithms as an adjunct radiative transfer code to deal with polarization effects.
© 2007 Elsevier Ltd. All rights reserved.

1. Introduction

Several radiative transfer (RT) models have been developed to compute the intensity and polarization of light reflected and/or transmitted by planetary atmospheres [1–5]. In remote sensing applications based on backscattered light measurements, calculations of multiple scattering with full treatment of polarization are computationally very expensive. Since multiple scattering is depolarizing, a low-order scattering

*Corresponding author. Tel.: +1 626 395 3992; fax: +1 626 585 1917.
E-mail address: vijay@gps.caltech.edu (V. Natraj).

0022-4073/$ - see front matter © 2007 Elsevier Ltd. All rights reserved.
doi:10.1016/j.jqsrt.2007.02.011

approximation is often used to compute the high-frequency Fourier components of the Stokes vector. Hovenier [6] developed analytic expressions, involving only angular integrations, to compute the first two orders of scattering for a homogeneous layer with polarization included. Kawabata and Ueno [7] used the invariant imbedding technique to compute the first three orders of scattering in vertically inhomogeneous plane–parallel layers. However, they neglected polarization.

In this paper, we extend the Kawabata and Ueno model to compute the first- and second-order reflection matrices for vertically inhomogeneous scattering media with polarization included. To enable accurate computations for the range of solar viewing angles encountered in nadir-view remote sensing applications, atmospheric transmittances for the incoming solar beam are treated for a curved spherical-shell atmosphere [8]. Polarization induces a change in the intensity; to account for this, we compute a correction to the scalar intensity. In this paper, we derive results for reflection, but it is straightforward to obtain analogous expressions for transmission. We also limit ourselves to a beam source of unpolarized incident light (e.g. sunlight).

For remote sensing inverse problems based on non-linear iterative fitting methods such as optimal estimation [9], the RT forward model should be able to generate both the simulated backscatter intensity and any number of associated weighting functions (partial derivatives of the intensity with respect to retrieved and other atmospheric and surface properties). In this regard, we have performed a complete linearization (analytic differentiation) of the two orders of scattering (2OS) model, both for the reflection matrix and for the intensity correction.

In this paper, we present the theoretical formulation for the simultaneous computation of the reflection matrix, the intensity correction and the corresponding weighting function fields. In Section 2, we summarize the invariant imbedding equations, and in Section 3, we derive the second-order scattering solutions with polarization. Section 4 deals with the linearization. In Section 5, we discuss aspects of the performance of our 2OS numerical RT code, and its validation. In Section 6, we present a series of results for an application based on measurements of reflected sunlight in the O_2 A band. In a subsequent paper, we will present further applications of the 2OS model for remote sensing retrievals [10].

2. Basic theory

2.1. Invariant imbedding analysis

We use the notation in [7], with additional terms to account for polarization. The Stokes vector $\boldsymbol{I}(\mu,\phi)$ of light reflected by a vertically inhomogeneous scattering–absorbing medium of optical thickness τ—measured from the bottom of the atmosphere (BOA)—can be expressed in terms of a reflection matrix $\mathbf{R}(\tau;-\mu,\mu_0,\phi-\phi_0)$:

$$\mathbf{I}(\mu,\phi) = \mu_0 \mathbf{R}(\tau;-\mu,\mu_0,\phi-\phi_0)\mathbf{F}_0, \tag{1}$$

where $\mathbf{F}_0$ is the Stokes vector of the incident radiation at the top of the atmosphere (TOA), $-\mu$ and μ_0 are the cosine of the viewing and incident zenith angles (with respect to the downward vertical) and $\phi-\phi_0$ is the relative azimuth angle between the viewing and incident directions. The azimuth dependence is expressed by means of a Fourier series expansion:

$$\begin{aligned}\mathbf{R}(\tau;-\mu,\mu_0,\phi-\phi_0) = {} & \mathbf{R}_1(\tau;-\mu,\mu_0,\phi-\phi_0) + \mathbf{R}^0_{2,c}(\tau;-\mu,\mu_0) \\ & + 2\sum_{m=1}^{M}[\mathbf{R}^m_{2,c}(\tau;-\mu,\mu_0)\cos\, m(\phi-\phi_0) + \mathbf{R}^m_{2,s}(\tau;-\mu,\mu_0)\sin\, m(\phi-\phi_0)],\end{aligned} \tag{2}$$

where the subscripts 1 and 2 refer to the order of scattering, while c and s refer to the cosine and sine components of the Fourier series, respectively. Aerosols and other scattering particles typically have a strong diffraction peak. On the other hand, multiple scattering tends to wash out strong scattering features. Hence, it is desirable to perform an exact computation of the single scattering for the particular viewing geometry; in Eq. (2), the exact first-order scattering contribution is determined separately. This is not only more accurate but also reduces the computational burden (see Section 5). M is the number of Fourier components necessary to achieve Fourier series convergence.

The intensity correction, $I_{\rm corr}$, is defined as:

$$I_{\rm corr}(\tau;-\mu,\mu_0,\phi-\phi_0) \equiv \mathbf{R}(\tau;-\mu,\mu_0,\phi-\phi_0)|_{(1,1)} - R(\tau;-\mu,\mu_0,\phi-\phi_0), \tag{3}$$

where $\mathbf{R}(\tau;-\mu,\mu_0,\phi-\phi_0)|_{(1,1)}$ is the (1,1) element of $\mathbf{R}(\tau;-\mu,\mu_0,\phi-\phi_0)$ and $R(\tau;-\mu,\mu_0,\phi-\phi_0)$ is the (scalar) reflection function. This can also be expanded in a Fourier series:

$$I_{\rm corr}(\tau;-\mu,\mu_0,\phi-\phi_0) = I^0_{\rm corr}(\tau;-\mu,\mu_0) + 2\sum_{m=1}^{M} I^m_{\rm corr}(\tau;-\mu,\mu_0)\cos m(\phi-\phi_0). \tag{4}$$

The expansion above does not involve sine terms because both the (1,1) element of the reflection matrix and the reflection function are even functions of the relative azimuth angle [1].

The first order of scattering does not contribute to the intensity correction, since for unpolarized incident light, the single scattered intensity is dependent only on the (1,1) element of the reflection matrix; the latter is the same with or without polarization. The sum of the intensity from a scalar multiple scattering calculation and the intensity correction computed above approximates the intensity with polarization included.

For $p \leqslant 2$, the contribution to the reflection matrix from the pth order of scattering, $\mathbf{R}_p$, obeys the integro-differential equation [1]:

$$\begin{aligned}\frac{\partial \mathbf{R}_p(\tau;-\mu,\mu_0,\phi-\phi_0)}{\partial\tau} = & -\left(\mu^{-1}+\lambda(z;\mu_0,\phi-\phi_0)\right)\mathbf{R}_p(\tau;-\mu,\mu_0,\phi-\phi_0)\\ & + \frac{\omega(\tau)}{4\pi\mu}\int_0^{2\pi}\int_0^1 \mathbf{P}(\tau;-\mu,-\mu',\phi-\phi')\mathbf{R}_{p-1}(\tau;-\mu',\mu_0,\phi'-\phi_0)\,\mathrm{d}\mu'\,\mathrm{d}\phi'\\ & + \frac{\omega(\tau)\lambda}{4\pi}\int_0^{2\pi}\int_0^1 \mathbf{R}_{p-1}(\tau;-\mu,\mu',\phi-\phi')\mathbf{P}(\tau;\mu',\mu_0,\phi'-\phi_0)\,\mathrm{d}\mu'\,\mathrm{d}\phi',\end{aligned} \tag{5}$$

where ω is the single scattering albedo, $\mathbf{P}$ is the phase matrix (see Section 2.2 for expressions to evaluate the phase matrix and its Fourier components), $\exp[-\lambda\tau]$ is the direct beam atmospheric transmittance factor and z is the altitude. Eq. (5) is valid in the pseudo-spherical approximation, where all scattering is regarded as taking place in a plane–parallel medium, but the solar beam attenuation is treated for a curved atmosphere. For a plane–parallel attenuation, $\lambda = 1/\mu_0$; in the curved atmosphere case, expressions for λ are derived in Section 3.1.

The various terms on the right hand side of Eq. (5) denote the following processes: direct transmission after p reflections, transmission (with illumination from below) after $p-1$ reflections and $p-1$ reflections after transmission. To calculate the transmission matrix, the only difference is that the last step in the photon history is downward. The equivalent processes would then be: direct transmission after p transmissions, transmission after $p-1$ transmissions and $p-1$ reflections (with illumination from below) after reflection.

Eq. (5) can be expanded in a Fourier series to obtain:

$$\frac{\partial \mathbf{R}^m_{p,\rm c}(\tau;-\mu,\mu_0)}{\partial\tau} = -\left(\mu^{-1}+\lambda\right)\mathbf{R}^m_{p,\rm c}(\tau;-\mu,\mu_0) + \mathbf{S}^m_{p,\rm c}(\tau;-\mu,\mu_0); \quad (p=1,2), \tag{6a}$$

$$\frac{\partial \mathbf{R}^m_{p,\rm s}(\tau;-\mu,\mu_0)}{\partial\tau} = -\left(\mu^{-1}+\lambda\right)\mathbf{R}^m_{p,\rm s}(\tau;-\mu,\mu_0) + \mathbf{S}^m_{p,\rm s}(\tau;-\mu,\mu_0); \quad (p=1,2), \tag{6b}$$

where the subscripts c and s refer to the cosine and sine Fourier components, and $\mathbf{S}^m_{p,\rm c}$ and $\mathbf{S}^m_{p,\rm s}$ are scattering source terms. The sine terms are identically zero for $m=0$. The first and second order scattering source terms are given by the following expressions:

$$\mathbf{S}^m_{1,\rm c}(\tau;-\mu,\mu_0) = \frac{\omega\lambda}{4\mu}\mathbf{P}^m_{\rm c}(\tau;-\mu,\mu_0), \tag{7a}$$

$$\mathbf{S}^m_{2,\mathrm{c}}(\tau;-\mu,\mu_0)=\frac{\omega}{2\mu}\int_0^1(\mathbf{P}^m_{\mathrm{c}}(\tau;-\mu,-\mu')\mathbf{R}^m_{1,\mathrm{c}}(\tau;-\mu',\mu_0)+\mathbf{P}^m_{\mathrm{s}}(\tau;-\mu,-\mu')\mathbf{R}^m_{1,\mathrm{s}}(\tau;-\mu',\mu_0))\,\mathrm{d}\mu'$$
$$+\frac{\omega\lambda}{2}\int_0^1(\mathbf{R}^m_{1,\mathrm{c}}(\tau;-\mu,\mu')\mathbf{P}^m_{\mathrm{c}}(\tau;\mu',\mu_0)-\mathbf{R}^m_{1,\mathrm{s}}(\tau;-\mu,\mu')\mathbf{P}^m_{\mathrm{s}}(\tau;\mu',\mu_0))\,\mathrm{d}\mu', \tag{7b}$$

$$\mathbf{S}^m_{1,\mathrm{s}}(\tau;-\mu,\mu_0)=\frac{\omega\lambda}{4\mu}\mathbf{P}^m_{\mathrm{s}}(\tau;-\mu,\mu_0), \tag{7c}$$

$$\mathbf{S}^m_{2,\mathrm{s}}(\tau;-\mu,\mu_0)=\frac{\omega}{2\mu}\int_0^1(\mathbf{P}^m_{\mathrm{c}}(\tau;-\mu,-\mu')\mathbf{R}^m_{1,\mathrm{s}}(\tau;-\mu',\mu_0)-\mathbf{P}^m_{\mathrm{s}}(\tau;-\mu,-\mu')\mathbf{R}^m_{1,\mathrm{c}}(\tau;-\mu',\mu_0))\,\mathrm{d}\mu'$$
$$+\frac{\omega\lambda}{2}\int_0^1(\mathbf{R}^m_{1,\mathrm{c}}(\tau;-\mu,\mu')\mathbf{P}^m_{\mathrm{s}}(\tau;\mu',\mu_0)+\mathbf{R}^m_{1,\mathrm{s}}(\tau;-\mu,\mu')\mathbf{P}^m_{\mathrm{c}}(\tau;\mu',\mu_0))\,\mathrm{d}\mu', \tag{7d}$$

where $\mathbf{P}^m_{\mathrm{c}}$ and $\mathbf{P}^m_{\mathrm{s}}$ are, respectively, the cosine and sine components of the mth term in the Fourier expansion of the phase matrix $\mathbf{P}$. Integrating Eqs. (6) over the optical depth from τ_n to τ, we obtain the following cosine and sine reflection matrices:

$$\mathbf{R}^m_{p,\mathrm{c}}(\tau;-\mu,\mu_0)=\mathbf{R}^m_{p,\mathrm{c}}(\tau_n;-\mu,\mu_0)\exp\left[-(\mu^{-1}+\lambda)(\tau-\tau_n)\right]$$
$$+\int_{\tau_n}^{\tau}\mathbf{S}^m_{p,\mathrm{c}}(t;-\mu,\mu_0)\exp\left[-(\mu^{-1}+\lambda)(\tau-t)\right]\mathrm{d}t;\quad(p=1,2), \tag{8a}$$

$$\mathbf{R}^m_{p,\mathrm{s}}(\tau;-\mu,\mu_0)=\mathbf{R}^m_{p,\mathrm{s}}(\tau_n;-\mu,\mu_0)\exp\left[-(\mu^{-1}+\lambda)(\tau-\tau_n)\right]$$
$$+\int_{\tau_n}^{\tau}\mathbf{S}^m_{p,\mathrm{s}}(t;-\mu,\mu_0)\exp\left[-(\mu^{-1}+\lambda)(\tau-t)\right]\mathrm{d}t;\quad(p=1,2). \tag{8b}$$

Starting from the scalar equivalent of Eq. (5), we can derive the Fourier components, $R^m_{p,\mathrm{c}}$, of the reflection functions, appropriate to the intensity correction:

$$R^m_{p,\mathrm{c}}(\tau;-\mu,\mu_0)=R^m_{p,\mathrm{c}}(\tau_n;-\mu,\mu_0)\exp\left[-(\mu^{-1}+\lambda)(\tau-\tau_n)\right]$$
$$+\int_{\tau_n}^{\tau}S^m_{p,\mathrm{c}}(t;-\mu,\mu_0)\exp\left[-(\mu^{-1}+\lambda)(\tau-t)\right]\mathrm{d}t;\quad(p=1,2), \tag{9}$$

where the source function terms are given by:

$$S^m_{1,\mathrm{c}}(\tau;-\mu,\mu_0)=\frac{\omega\lambda}{4\mu}P^m_{\mathrm{c}}(\tau;-\mu,\mu_0), \tag{10a}$$

$$S^m_{2,\mathrm{c}}(\tau;-\mu,\mu_0)=\frac{\omega}{2\mu}\int_0^1P^m_{\mathrm{c}}(\tau;-\mu,-\mu')R^m_{1,\mathrm{c}}(\tau;-\mu',\mu_0)\,\mathrm{d}\mu'+\frac{\omega\lambda}{2}\int_0^1R^m_{1,\mathrm{c}}(\tau;-\mu,\mu')P^m_{\mathrm{c}}(\tau;\mu',\mu_0)\,\mathrm{d}\mu'. \tag{10b}$$

P^m_{c} is the mth term in the Fourier expansion of the phase function. The Fourier components of the intensity correction can then be approximated as:

$$I^m_{\mathrm{corr}}(\tau;-\mu,\mu_0)=\mathbf{R}^m_{2,\mathrm{c}}(\tau;-\mu,\mu_0)\big|_{(1,1)}-R^m_{2,\mathrm{c}}(\tau;-\mu,\mu_0), \tag{11}$$

where $\mathbf{R}^m_{2,\mathrm{c}}(\tau;-\mu,\mu_0)|_{(1,1)}$ is the (1,1) element of $\mathbf{R}^m_{2,\mathrm{c}}(\tau;-\mu,\mu_0)$.

In Eqs. (7)–(10), all integrals over the polar direction half-spaces are approximated by summations using Gaussian quadrature [11]. The quadrature has N_{g} points, with abscissae and weights $\{\pm\mu_k,w_k\}$, $k=1,\ldots,N_{\mathrm{g}}$, in the upwelling and downwelling polar hemispheres.

2.2. Expansion of the phase matrix

We divide the atmosphere into N horizontally homogeneous layers ($N+1$ levels), where the TOA is the $N+1$th level. The optical properties are assumed to be constant within a layer. We then define the symbol $\mathbf{\Omega}_n$

to indicate the sun–satellite geometry appropriate to a given layer n:

$$\mathbf{\Omega}_n = (\vartheta_n, \alpha_n, \varphi_n), \tag{12}$$

where ϑ_n, α_n and φ_n are the local solar zenith angle, the local line of sight zenith angle and the local relative azimuth angle between two planes containing these directions, respectively, at the bottom boundary of layer n. Ray tracing in a curved atmosphere (with or without refraction) may be used to determine all $\mathbf{\Omega}_n$ given the input geometry at the TOA. In the pseudo-spherical approximation, all scattering is considered to be in a plane–parallel atmosphere; only the solar beam attenuation is treated for spherical curvature. In this case, $\mathbf{\Omega}_n = (\cos^{-1}\mu_0, \cos^{-1}(-\mu), \phi - \phi_0)$ for all points along the upward nadir from the BOA. The scattering angle Θ_n can be computed using spherical trigonometry:

$$\cos\Theta_n = \cos\vartheta_n \cos\alpha_n + \sin\vartheta_n \sin\alpha_n \cos\varphi_n. \tag{13}$$

For a non-refracting atmosphere, the scattering angle is a constant and is given by the value at the TOA:

$$\cos\,\Theta_n = -\mu_0\mu + \sqrt{1-\mu_0^2}\sqrt{1-\mu^2}\cos(\phi - \phi_0). \tag{14}$$

For scattering matrices where the elements are functions only of the scattering angle, and where there are at most six independent elements [1], the scattering matrix expansion is given in terms of a set of generalized spherical functions $S^l_{m,n}(\cos\,\Theta_n)$ [12]. The six independent elements are:

$$a_1(\Theta_n) = \sum_{l=0}^{L} \beta_{nl} S^l_{0,0}(\cos\,\Theta_n), \tag{15a}$$

$$a_2(\Theta_n) + a_3(\Theta_n) = \sum_{l=0}^{L} (\alpha_{nl} + \zeta_{nl}) S^l_{2,2}(\cos\,\Theta_n), \tag{15b}$$

$$a_2(\Theta_n) - a_3(\Theta_n) = \sum_{l=0}^{L} (\alpha_{nl} - \zeta_{nl}) S^l_{2,-2}(\cos\,\Theta_n), \tag{15c}$$

$$a_4(\Theta_n) = \sum_{l=0}^{L} \delta_{nl} S^l_{0,0}(\cos\,\Theta_n), \tag{15d}$$

$$b_1(\Theta_n) = \sum_{l=0}^{L} \gamma_{nl} S^l_{0,2}(\cos\,\Theta_n), \tag{15e}$$

$$b_2(\Theta_n) = -\sum_{l=0}^{L} \varepsilon_{nl} S^l_{0,2}(\cos\,\Theta_n). \tag{15f}$$

There are six sets of expansion coefficients $\{\alpha_{nl},\beta_{nl},\gamma_{nl},\delta_{nl},\varepsilon_{nl},\zeta_{nl}\}$, where $\{\beta_{nl}\}$ are the phase function Legendre expansion coefficients as required for scalar-only computations neglecting polarization. The functions $\{a_1,a_2,a_3,a_4\}$ and $\{b_1,b_2\}$ are elements of the scattering matrix $\mathbf{F}_n$:

$$\mathbf{F}_n(\Theta_n) = \begin{pmatrix} a_1(\Theta_n) & b_1(\Theta_n) & 0 & 0 \\ b_1(\Theta_n) & a_2(\Theta_n) & 0 & 0 \\ 0 & 0 & a_3(\Theta_n) & b_2(\Theta_n) \\ 0 & 0 & -b_2(\Theta_n) & a_4(\Theta_n) \end{pmatrix}. \tag{16}$$

The corresponding expansion coefficient matrix $\mathbf{B}_{nl}$ is:

$$\mathbf{B}_{nl} = \begin{pmatrix} \beta_{nl} & \gamma_{nl} & 0 & 0 \\ \gamma_{nl} & \alpha_{nl} & 0 & 0 \\ 0 & 0 & \varsigma_{nl} & -\varepsilon_{nl} \\ 0 & 0 & \varepsilon_{nl} & \delta_{nl} \end{pmatrix}. \tag{17}$$

The Stokes vector is defined with respect to a reference plane (usually taken to be the local meridian plane). To transform the Stokes vectors from the scattering plane to the local meridian planes containing the incident and scattered beams, we need rotation matrices $\mathbf{L}(\pi-\sigma_2)$ and $\mathbf{L}(\pi-\sigma_1)$, where σ_1 and σ_2 are the angles of rotation [12]. The phase matrix $\mathbf{\Pi}_n(\mathbf{\Omega}_n)$ is then given by:

$$\mathbf{\Pi}_n(\mathbf{\Omega}_n) = \mathbf{L}(\pi - \sigma_2)\mathbf{F}_n(\Theta_n)\mathbf{L}(-\sigma_1). \tag{18}$$

The phase matrix can be decomposed into its Fourier components [13]:

$$\mathbf{P}(-\mu, \pm\mu', \phi - \phi') = \mathbf{P}_{\mathrm{c}}^0(-\mu, \pm\mu') + 2\sum_{m=1}^{M}[\mathbf{P}_{\mathrm{c}}^m(-\mu, \pm\mu')\cos\, m(\phi - \phi') + \mathbf{P}_{\mathrm{s}}^m(-\mu, \pm\mu')\sin\, m(\phi - \phi')], \tag{19a}$$

$$\mathbf{P}(\pm\mu', \mu_0, \phi' - \phi_0) = \mathbf{P}_{\mathrm{c}}^0(\pm\mu', \mu_0) + 2\sum_{m=1}^{M}[\mathbf{P}_{\mathrm{c}}^m(\pm\mu', \mu_0)\cos\, m(\phi' - \phi_0) + \mathbf{P}_{\mathrm{s}}^m(\pm\mu', \mu_0)\sin\, m(\phi' - \phi_0)], \tag{19b}$$

$$\mathbf{P}(-\mu, \mu_0, \phi - \phi_0) = \mathbf{P}_{\mathrm{c}}^0(-\mu, \mu_0) + 2\sum_{m=1}^{M}[\mathbf{P}_{\mathrm{c}}^m(-\mu, \mu_0)\cos\, m(\phi - \phi_0) + \mathbf{P}_{\mathrm{s}}^m(-\mu, \mu_0)\sin\, m(\phi - \phi_0)]. \tag{19c}$$

The full phase matrix (with an exact specification of the scattering law) will be used to calculate the exact first order scattering term, while the truncated form of the phase matrix using the Fourier component expansion in Eqs. (19) will be used for computing the second order of scattering.

$\mathbf{P}_{\mathrm{c}}^m$ and $\mathbf{P}_{\mathrm{s}}^m$ are given by:

$$\mathbf{P}_{\mathrm{c}}^m(\mu_i, \mu_j) = \mathbf{A}^m(\mu_i, \mu_j) + \mathbf{D}\mathbf{A}^m(\mu_i, \mu_j)\mathbf{D}, \tag{20a}$$

$$\mathbf{P}_{\mathrm{s}}^m(\mu_i, \mu_j) = \mathbf{A}^m(\mu_i, \mu_j)\mathbf{D} - \mathbf{D}\mathbf{A}^m(\mu_i, \mu_j), \tag{20b}$$

$$\mathbf{A}^m(\mu_i, \mu_j) = \sum_{l=m}^{M} \mathbf{\Pi}_l^m(\mu_i)\mathbf{B}_l^m\mathbf{\Pi}_l^m(\mu_j), \tag{20c}$$

$$\mathbf{D} = diag\,\{1, 1, -1, -1\}, \tag{20d}$$

$$\mathbf{\Pi}_l^m(\mu) = \begin{pmatrix} P_l^m(\mu) & 0 & 0 & 0 \\ 0 & R_l^m(\mu) & -T_l^m(\mu) & 0 \\ 0 & -T_l^m(\mu) & R_l^m(\mu) & 0 \\ 0 & 0 & 0 & P_l^m(\mu) \end{pmatrix}, \tag{20e}$$

$$\mathbf{B}_l^m = \frac{(l-m)!}{(l+m)!}\mathbf{B}_{nl}, \tag{20f}$$

where $\mu_i = -\mu, \pm\mu'$ and $\mu_j = \pm\mu', \mu_0$.

The $\mathbf{\Pi}_l^m$ matrices contain entries of normalized Legendre functions P_l^m and functions R_l^m and T_l^m, which are related to the generalized spherical functions [13].

3. Solution for the first two orders of scattering

3.1. Solar beam attenuation in a curved atmosphere

The assumption of a plane–parallel medium breaks down for solar zenith angles and/or line of sight viewing angles approaching 90°; it then becomes necessary to make some allowance for the sphericity of the atmosphere. This is particularly important for polar-orbiting satellite instruments, for which large solar zenith angles are frequently encountered. In a stratified spherical-shell medium, the intensity field changes with angular variables (solar and line of sight zenith angles, relative azimuth angle between planes containing the line of sight and solar directions) in addition to the zenith variation with optical depth. The pseudo-spherical assumption ignores these angular derivatives; only the variation of intensity with the vertical coordinate is considered.

In a plane–parallel atmosphere, the direct beam attenuation is given by $\exp[-\tau/\mu_0]$. In a spherical-shell atmosphere, the attenuation factor is $\exp[-\kappa(\tau)]$, where κ is the slant optical depth. The cumulative slant optical depth κ_n to the bottom boundary of layer n can be expressed as:

$$\kappa_n = \sum_{k=N}^{n} \kappa_{nk} = \sum_{k=N}^{n} s_{nk} e_k, \tag{21}$$

where κ_{nk} are the slant optical thickness values for layers k above and equal to n, and s_{nk} and e_k are the layer path lengths and layer extinctions respectively. For straight-line paths, the path lengths may be expressed easily in terms of vertical altitudes. In a refractive atmosphere, they can be calculated by repeated application of Snell's law. Slant path transmittances are taken to be exact at layer boundaries, with a simple exponential in optical thickness to approximate the attenuation across layers [8]

$$\lambda_n = \frac{\kappa_n - \kappa_{n+1}}{\tau_{n+1} - \tau_n} = \frac{1}{\tau_{n+1} - \tau_n} \left[\sum_{k=N}^{N+1-n} s_{nk} e_k - \sum_{k=N}^{N+2-n} s_{(n+1)k} e_k \right]. \tag{22}$$

For a curved atmosphere, the layer-specific "average secant" λ_n takes the place of the solar cosine secant; in the plane–parallel case, we have $\lambda_n = \mu_0^{-1}$ for all n. In a pseudo-spherical RT model, scattering takes place along the local vertical from the BOA point. It has been shown [14,15] that the pseudo-spherical approximation provides a useful and sufficiently accurate RT intensity simulation for solar zenith angles up to 90°, provided that the line of sight is reasonably close to the nadir. The advantage of this approach is that it utilizes the speed and flexibility of the plane–parallel formalism, and avoids the more complex and computationally intensive full spherical RT treatment.

In the following exposition, we have stayed with the notation used in [7], with some changes to account for the pseudo-spherical treatment. For simplicity, we have assumed a non-refractive atmosphere.

3.2. First-order scattering

We define the following functions:

$$\Psi(\tau_{n+1}; y) \equiv \exp[-y(\tau_{n+1} - \tau_n)]. \tag{23}$$

$$\Phi(\tau_{n+1}; \alpha, \beta, \gamma) \equiv \left\{ \begin{array}{ll} \frac{\Psi(\tau_{n+1};\alpha+\gamma) - \Psi(\tau_{n+1};\beta+\gamma)}{\beta-\alpha}, & \beta \neq \alpha \\ (\tau_{n+1} - \tau_n)\Psi(\tau_{n+1}; \alpha+\gamma), & \beta = \alpha \end{array} \right\}. \tag{24}$$

We also define:

$$x' \equiv \frac{1}{\mu'}. \tag{25}$$

Layer dependence of the optical depth, single scattering albedo and phase matrix decomposition is implicit. The expressions below reduce to those derived by Hovenier [6] for the case of a plane–parallel single-layer medium.

The cosine and sine terms for the first order of scattering are given below:

$$\mathbf{R}^m_{1,\mathrm{c}}(\tau_{n+1};-\mu,\mu') = \mathbf{R}^m_{1,\mathrm{c}}(\tau_n;-\mu,\mu')\Psi(\tau_{n+1};\mu^{-1}+x') + \frac{\omega_n\mu^{-1}x'}{4(\mu^{-1}+x')}\left[1-\Psi(\tau_{n+1};\mu^{-1}+x')\right]\mathbf{P}^m_{\mathrm{c}}(-\mu,\mu'), \tag{26a}$$

$$\mathbf{R}^m_{1,\mathrm{c}}(\tau_{n+1};-\mu',\mu_0) = \mathbf{R}^m_{1,\mathrm{c}}(\tau_n;-\mu',\mu_0)\Psi(\tau_{n+1};x'+\lambda_n) + \frac{\omega_n x'\lambda_n}{4(x'+\lambda_n)}[1-\Psi(\tau_{n+1};x'+\lambda_n)]\mathbf{P}^m_{\mathrm{c}}(-\mu',\mu_0), \tag{26b}$$

$$\mathbf{R}^m_{1,\mathrm{s}}(\tau_{n+1};-\mu,\mu') = \mathbf{R}^m_{1,\mathrm{s}}(\tau_n;-\mu,\mu')\Psi(\tau_{n+1};\mu^{-1}+x') + \frac{\omega_n\mu^{-1}x'}{4(\mu^{-1}+x')}\left[1-\Psi(\tau_{n+1};\mu^{-1}+x')\right]\mathbf{P}^m_{\mathrm{s}}(-\mu,\mu'), \tag{27a}$$

$$\mathbf{R}^m_{1,\mathrm{s}}(\tau_{n+1};-\mu',\mu_0) = \mathbf{R}^m_{1,\mathrm{s}}(\tau_n;-\mu',\mu_0)\Psi(\tau_{n+1};x'+\lambda_n) + \frac{\omega_n x'\lambda_n}{4(x'+\lambda_n)}[1-\Psi(\tau_{n+1};x'+\lambda_n)]\mathbf{P}^m_{\mathrm{s}}(-\mu',\mu_0). \tag{27b}$$

For the intensity correction, we have the following contributions:

$$R^m_{1,\mathrm{c}}(\tau_{n+1};-\mu,\mu') = R^m_{1,\mathrm{c}}(\tau_n;-\mu,\mu')\Psi(\tau_{n+1};\mu^{-1}+x') + \frac{\omega_n\mu^{-1}x'}{4(\mu^{-1}+x')}\left[1-\Psi(\tau_{n+1};\mu^{-1}+x')\right]P^m_{\mathrm{c}}(-\mu,\mu'), \tag{28a}$$

$$R^m_{1,\mathrm{c}}(\tau_{n+1};-\mu',\mu_0) = R^m_{1,\mathrm{c}}(\tau_n;-\mu',\mu_0)\Psi(\tau_{n+1};x'+\lambda_n) + \frac{\omega_n x'\lambda_n}{4(x'+\lambda_n)}[1-\Psi(\tau_{n+1};x'+\lambda_n)]P^m_{\mathrm{c}}(-\mu',\mu_0). \tag{28b}$$

The above expressions refer to the first-order terms that arise during the computation of the second order of scattering. The exact first-order computation will be done separately in Section 3.4.

3.3. Second-order scattering

Similar expressions pertain to the second order scattering. The cosine terms are given by:

$$\begin{aligned}\mathbf{R}^m_{2,\mathrm{c}}(\tau_{n+1};-\mu,\mu_0) = {}& \mathbf{R}^m_{2,\mathrm{c}}(\tau_n;-\mu,\mu_0)\Psi(\tau_{n+1};\mu^{-1}+\lambda_n) + \frac{\omega_n}{2\mu}\int_0^1 \mathbf{P}^m_{\mathrm{c}}(-\mu,-\mu')\mathbf{V}^m_1(-\mu',\mu_0)\,\mathrm{d}\mu' \\ & + \frac{\omega_n}{2\mu}\int_0^1 \mathbf{P}^m_{\mathrm{s}}(-\mu,-\mu')\mathbf{V}^m_2(-\mu',\mu_0)\,\mathrm{d}\mu' + \frac{\omega_n\lambda_n}{2}\int_0^1 \mathbf{V}^m_3(-\mu,\mu')\mathbf{P}^m_{\mathrm{c}}(\mu',\mu_0)\,\mathrm{d}\mu' \\ & - \frac{\omega_n\lambda_n}{2}\int_0^1 \mathbf{V}^m_4(-\mu,\mu')\mathbf{P}^m_{\mathrm{s}}(\mu',\mu_0)\,\mathrm{d}\mu',\end{aligned} \tag{29a}$$

where:

$$\begin{aligned}\mathbf{V}^m_1(-\mu',\mu_0) = {}& \Phi(\tau_{n+1};\mu^{-1},x',\lambda_n)\mathbf{R}^m_{1,\mathrm{c}}(\tau_n;-\mu',\mu_0) + \frac{\mathbf{P}^m_{\mathrm{c}}(-\mu',\mu_0)\omega_n x'\lambda_n}{4(x'+\lambda_n)(\mu^{-1}+\lambda_n)} \\ & \times\left[1-\Psi(\tau_{n+1};\mu^{-1}+\lambda_n)-(\mu^{-1}+\lambda_n)\Phi(\tau_{n+1};\mu^{-1},x',\lambda_n)\right],\end{aligned} \tag{29b}$$

$$\begin{aligned}\mathbf{V}^m_2(-\mu',\mu_0) = {}& \Phi(\tau_{n+1};\mu^{-1},x',\lambda_n)\mathbf{R}^m_{1,\mathrm{s}}(\tau_n;-\mu',\mu_0) + \frac{\mathbf{P}^m_{\mathrm{s}}(-\mu',\mu_0)\,\omega_n x'\lambda_n}{4(x'+\lambda_n)(\mu^{-1}+\lambda_n)} \\ & \times\left[1-\Psi(\tau_{n+1};\mu^{-1}+\lambda_n)-(\mu^{-1}+\lambda_n)\Phi(\tau_{n+1};\mu^{-1},x',\lambda_n)\right],\end{aligned} \tag{29c}$$

$$\mathbf{V}_3^m(-\mu,\mu') = \Phi(\tau_{n+1};x',\lambda_n,\mu^{-1})\mathbf{R}_{1,c}^m(\tau_n;-\mu,\mu') + \frac{\mathbf{P}_c^m(-\mu,\mu')\omega_n x'\mu^{-1}}{4(\mu^{-1}+\lambda_n)(x'+\mu^{-1})} \times \left[1-\Psi(\tau_{n+1};\mu^{-1}+\lambda_n) - (\mu^{-1}+\lambda_n)\Phi(\tau_{n+1};x',\lambda_n,\mu^{-1})\right], \tag{29d}$$

$$\mathbf{V}_4^m(-\mu,\mu') = \Phi(\tau_{n+1};x',\lambda_n,\mu^{-1})\mathbf{R}_{1,s}^m(\tau_n;-\mu,\mu') + \frac{\mathbf{P}_s^m(-\mu,\mu')\omega_n x'\mu^{-1}}{4(\mu^{-1}+\lambda_n)(x'+\mu^{-1})}\left[1-\Psi(\tau_{n+1};\mu^{-1}+\lambda_n) - (\mu^{-1}+\lambda_n)\Phi(\tau_{n+1};x',\lambda_n,\mu^{-1})\right]. \tag{29e}$$

The sine-series contributions to the second-order scattering are:

$$\mathbf{R}_{2,s}^m(\tau_{n+1};-\mu,\mu_0) = \mathbf{R}_{2,s}^m(\tau_n;-\mu,\mu_0)\Psi(\tau_{n+1};\mu^{-1}+\lambda_n) + \frac{\omega_n}{2\mu}\int_0^1 \mathbf{P}_c^m(-\mu,-\mu')\mathbf{V}_2^m(-\mu',\mu_0)\,\mathrm{d}\mu' - \frac{\omega_n}{2\mu}\int_0^1 \mathbf{P}_s^m(-\mu,-\mu')\mathbf{V}_1^m(-\mu',\mu_0)\,\mathrm{d}\mu' + \frac{\omega_n\lambda_n}{2}\int_0^1 \mathbf{V}_3^m(-\mu,\mu')\mathbf{P}_s^m(\mu',\mu_0)\,\mathrm{d}\mu' + \frac{\omega_n\lambda_n}{2}\int_0^1 \mathbf{V}_4^m(-\mu,\mu')\mathbf{P}_c^m(\mu',\mu_0)\,\mathrm{d}\mu'. \tag{30}$$

Lastly, we have the reflection functions for the intensity correction:

$$R_{2,c}^m(\tau_{n+1};-\mu,\mu_0) = R_{2,c}^m(\tau_n;-\mu,\mu_0)\Psi(\tau_{n+1};\mu^{-1}+\lambda_n) + \frac{\omega_n}{2\mu}\int_0^1 P_c^m(-\mu,-\mu')V_1^m(-\mu',\mu_0)\,\mathrm{d}\mu' + \frac{\omega_n\lambda_n}{2}\int_0^1 V_3^m(-\mu,\mu')P_c^m(\mu',\mu_0)\,\mathrm{d}\mu', \tag{31a}$$

$$V_1^m(-\mu',\mu_0) = \Phi(\tau_{n+1};\mu^{-1},x',\lambda_n)R_{1,c}^m(\tau_n;-\mu',\mu_0) + \frac{P_c^m(-\mu',\mu_0)\omega_n x'\lambda_n}{4(x'+\lambda_n)(\mu^{-1}+\lambda_n)} \times \left[1-\Psi(\tau_{n+1};\mu^{-1}+\lambda_n) - (\mu^{-1}+\lambda_n)\Phi(\tau_{n+1};\mu^{-1},x',\lambda_n)\right], \tag{31b}$$

$$V_3^m(-\mu,\mu') = \Phi(\tau_{n+1};x',\lambda_n,\mu^{-1})R_{1,c}^m(\tau_n;-\mu,\mu') + \frac{P_c^m(-\mu,\mu')\omega_n x'\mu^{-1}}{4(\mu^{-1}+\lambda_n)(x'+\mu^{-1})} \times \left[1-\Psi(\tau_{n+1};\mu^{-1}+\lambda_n) - (\mu^{-1}+\lambda_n)\Phi(\tau_{n+1};x',\lambda_n,\mu^{-1})\right]. \tag{31c}$$

The Fourier components of the intensity correction at the TOA can be obtained from Eqs. (11), (29) and (31):

$$I_{\mathrm{corr}}^m(\tau_{N+1}) = \mathbf{R}_{2,c}^m(\tau_{N+1};-\mu,\mu_0)|_{(1,1)} - R_{2,c}^m(\tau_{N+1};-\mu,\mu_0). \tag{32}$$

3.4. Exact solution for first-order scattering

In this case, the reflection matrix at the top of layer n is based on an exact single scatter source term:

$$\mathbf{R}_1(\tau_{n+1};\mathbf{\Omega}_{n+1}) = \mathbf{R}_1(\tau_n;\mathbf{\Omega}_n)\Psi(\tau_{n+1};\mu^{-1}+\lambda_n) + \frac{\omega_n\mu^{-1}\lambda_n}{4(\mu^{-1}+\lambda_n)}\left[1-\Psi(\tau_{n+1};\mu^{-1}+\lambda_n)\right]\mathbf{\Pi}_n(\mathbf{\Omega}_n). \tag{33}$$

Here, the phase matrix $\mathbf{\Pi}_n(\mathbf{\Omega}_n)$ is evaluated using an exact specification of the scattering law based on the use of complete sets of expansion coefficients (cf. Section 2.2).

3.5. Boundary conditions

The recurrence relations in Sections 3.3 and 3.4 all start with values of the reflection matrices at the surface. The surface boundary condition requires a complete specification of the first-order bidirectional reflection distribution function (BRDF) at the surface; second order of scattering reflection functions are zero. Thus we have:

$$\mathbf{R}_{1,c}^m(0;-\mu,\mu') = \mathbf{R}_{g,c}^m(-\mu,\mu'), \tag{34a}$$

$$\mathbf{R}^m_{1,c}(0;-\mu',\mu_0) = \mathbf{R}^m_{g,c}(-\mu',\mu_0), \tag{34b}$$

$$\mathbf{R}^m_{1,s}(0;-\mu,\mu') = \mathbf{R}^m_{g,s}(-\mu,\mu'), \tag{34c}$$

$$\mathbf{R}^m_{1,s}(0;-\mu',\mu_0) = \mathbf{R}^m_{g,s}(-\mu',\mu_0), \tag{34d}$$

$$\mathbf{R}^m_{2,c}(0;-\mu,\mu_0) = 0, \tag{34e}$$

$$\mathbf{R}^m_{2,s}(0;-\mu,\mu_0) = 0, \tag{34f}$$

$$\mathbf{R}_1(0;\mathbf{\Omega}_0) = \mathbf{R}_g(\mathbf{\Omega}_0), \tag{34g}$$

where $\mathbf{R}_g$ is the surface BRDF, and $\mathbf{\Omega}_0$ is given by the following expression:

$$\mathbf{\Omega}_0 = \{(\arccos(\mu_0), \arccos(-\mu), \phi - \phi_0)\}. \tag{35}$$

Two commonly encountered surface types are Lambertian and ocean sun glint. The Lambertian BRDF is (A_g is the Lambertian albedo):

$$\mathbf{R}_g(\mathbf{\Omega}_0) = A_g \begin{pmatrix} 1 & 0 & 0 & 0 \\ 0 & 0 & 0 & 0 \\ 0 & 0 & 0 & 0 \\ 0 & 0 & 0 & 0 \end{pmatrix}. \tag{36}$$

We compute the ocean sun glint BRDF using a modified Kirchhoff approximation [16] based on an isotropic Gaussian probability distribution of wave-facet slopes:

$$F(\alpha,\phi) = \frac{1}{2\pi s^2}\exp\left[-\frac{\alpha^2}{2s^2(1-\alpha^2)}\right], \tag{37}$$

where the mean square slope s^2 is related to the near-surface wind speed W (in m/s) by the following well-known empirical formula [17]:

$$2s^2 = 0.003 + 0.00512\,W. \tag{38}$$

Shadowing by surface waves is taken into account using a symmetrical bidirectional shadowing function $S(\alpha,\beta)$ for facet incident and reflected normal angles α and β [18]:

$$S(\alpha,\beta) = \frac{1}{1+\Lambda(\alpha)+\Lambda(\beta)}, \tag{39a}$$

where:

$$\Lambda(\alpha) = \frac{1}{2}\left(\left[\frac{2(1-\alpha^2)}{\pi}\right]^{1/2}\frac{s}{\alpha}\exp\left[-\frac{\alpha^2}{2s^2(1-\alpha^2)}\right] - \mathrm{erfc}\left[\frac{\alpha}{s\sqrt{2(1-\alpha^2)}}\right]\right). \tag{39b}$$

Here, erfc(x) is the complementary error function. Fourier components of the ocean sun glint BRDF, $\mathbf{R}^m_{g,c}$ and $\mathbf{R}^m_{g,s}$, are obtained by Gaussian quadrature. Details of the ocean surface reflection matrix computation are described in Ref. [18].

4. Linearization

In remote sensing inverse problems, it is usually necessary for the forward model to be able to generate sensitivity (or weighting) functions, *i.e.*, partial derivatives of the simulated radiance field with respect to atmospheric and surface parameters that are retrieved or are sources of error in the retrieval. In this paper, we use the term "linearization" as a synonym for analytic differentiation of the radiation field. We distinguish between weighting functions defined with respect to atmospheric variables (Section 4.1), and those defined with respect to surface variables (Section 4.2).

4.1. Atmospheric profile linearization

We define the linearization operator with respect to some variable ξ_k in layer k as follows:

$$L_k \equiv \frac{\partial}{\partial \xi_k}. \tag{40}$$

The 2OS model requires as input the layer optical thickness values, $\Delta_n = \tau_{n-1} - \tau_n$, the total single scattering albedos ω_n and the matrix $\mathbf{B}_{nl}$ of expansion coefficients in Eq. (17). These are the inherent optical properties (IOPs). For the linearization, we require the set of derivative or linearized inputs:

$$u_n \equiv L_n[\omega_n], \quad v_n \equiv L_n[\Delta_n], \quad \mathbf{z}_{nl} \equiv L_n[\mathbf{B}_{nl}]. \tag{41}$$

The IOPS and their linearizations in Eq. (41) are the end points in the chain-rule differentiation of the reflection matrices.

We note that for a variable ξ_k in layer k there are no derivatives in layers above k; in other words, $L_k[Q_n] = 0, \forall_n > k$ for any quantity Q_n defined in layer n (layers are numbered from the surface upwards). In the pseudo-spherical treatment, derivatives of the solar beam secant factors $L_k[\lambda_n] \equiv \sigma_{nk}$ may be found by differentiating Eq. (22); for details of this procedure, see *e.g.,* Ref. [3]. For plane–parallel attenuation, $\sigma_{nk} = 0, \forall n,k$, since $\lambda_n = \mu_0^{-1}$.

The linearization of the complete second-order fields is a straightforward exercise based on repeated chain-rule differentiation. Here, we derive the results for the exact single-scatter reflection functions (*cf.* Section 3.4); the analysis for the second-order functions and the intensity correction may be found in Appendix A.

For the exact first-order reflection matrix terms, we first rewrite Eq. (33) as:

$$\mathbf{R}_1(L_{n+1}, \mathbf{\Omega}_{n+1}) = \mathbf{R}_1(L_n, \mathbf{\Omega}_n) Q_n(\mu, \lambda_n) + \omega_n E_n(\mu, \lambda_n) \mathbf{\Pi}_n(\mathbf{\Omega}_n), \tag{42}$$

where L_{n+1} is the top of layer n. In Eq. (42), we have:

$$Q_n(\mu, \lambda_n) = \mathrm{e}^{-(\tau_{n+1} - \tau_n)(\mu^{-1} + \lambda_n)}, \tag{43a}$$

$$E_n(\mu, \lambda_n) = \frac{\mu^{-1}\lambda_n}{4(\mu^{-1} + \lambda_n)} \left[1 - Q_n(\mu, \lambda_n)\right]. \tag{43b}$$

Eq. (42) can now be differentiated:

$$L_k[\mathbf{R}_1(L_{n+1}, \mathbf{\Omega}_{n+1})] = L_k[\mathbf{R}_1(L_n, \mathbf{\Omega}_n)] Q_n(\mu, \lambda_n) + \mathbf{R}_1(L_n, \mathbf{\Omega}_n) L_k[Q_n(\mu, \lambda_n)] + L_k[\omega_n E_n(\mu, \lambda_n) \mathbf{\Pi}_n(\mathbf{\Omega}_n)]. \tag{44}$$

We note that:

$$L_k[Q_n(\mu, \lambda_n)] = -Q_n(\mu, \lambda_n)[(\mu^{-1} + \lambda_n) v_n \delta_{nk} + \Delta_n \sigma_{nk}] \equiv H_{nk}(\mu, \lambda_n), \tag{45}$$

$$L_k[\omega_n] = u_n \delta_{nk}, \tag{46}$$

$$L_k[\mathbf{\Pi}_n(\mathbf{\Omega}_n)] = f(\mathbf{z}_{nl}) \delta_{nk} \equiv \mathbf{\psi}_{nk}, \tag{47}$$

$$\begin{aligned} L_k[E_n(\mu, \lambda_n)] &= \left(\frac{\mu^{-1}\sigma_{nk}}{4(\mu^{-1} + \lambda_n)} - \frac{\mu^{-1}\lambda_n \sigma_{nk}}{4(\mu^{-1} + \lambda_n)^2} \right) (1 - Q_n(\mu, \lambda_n)) - \frac{\mu^{-1}\lambda_n H_{nk}(\mu, \lambda_n)}{4(\mu^{-1} + \lambda_n)} \\ &= \frac{\mu^{-2}\sigma_{nk}(1 - Q_n(\mu, \lambda_n))}{4(\mu^{-1} + \lambda_n)^2} - \frac{\mu^{-1}\lambda_n H_{nk}(\mu, \lambda_n)}{4(\mu^{-1} + \lambda_n)} \equiv F_{nk}(\mu, \lambda_n). \end{aligned} \tag{48}$$

Here, δ_{nk} is the Kronecker delta function. In Eq. (47), the phase matrix can be expressed in terms of input expansion coefficients $\mathbf{B}_{nl}$ (*cf.* Eqs. (15)–(18)), so its linearization will be a known function $f(\mathbf{z}_{nl})$ of the IOP coefficient derivatives $\mathbf{z}_{nl}$.

With the help of the above auxiliary definitions, Eq. (44) can now be written as:

$$\begin{aligned} L_k[\mathbf{R}_1(L_{n+1}, \mathbf{\Omega}_{n+1})] = {} & L_k[\mathbf{R}_1(L_n, \mathbf{\Omega}_n)] Q_n(\mu, \lambda_n) + \mathbf{R}_1(L_n, \mathbf{\Omega}_n) H_{nk}(\mu, \lambda_n) + \omega_n E_n(\mu, \lambda_n) \mathbf{\psi}_{nk} \\ & + \mathbf{\Pi}_n(\mathbf{\Omega}_n)[F_{nk}(\mu, \lambda_n)\omega_n + E_n(\mu, \lambda_n) u_n \delta_{nk}]. \end{aligned} \tag{49}$$

4.2. Surface property linearization

Let η be a surface property for which we wish to find the weighting function. In our case, η is either the albedo for a Lambertian surface or the wind speed for an ocean sun glint surface. We define the surface linearization operator as follows:

$$L_\eta \equiv \frac{\partial}{\partial \eta}. \tag{50}$$

The atmospheric profile IOPs do not depend on η, so atmospheric scattering source terms will have no derivatives with respect to this variable. Thus, linearization of reflection matrices with respect to η will propagate upwards from the derivatives of the surface BRDFs with respect to η. The linearized surface boundary condition can be written as:

$$L_\eta[\mathbf{R}^m_{1,\mathrm{c}}(0;-\mu,\mu')] = L_\eta[\mathbf{R}^m_{\mathrm{g,c}}(-\mu,\mu')], \tag{51a}$$

$$L_\eta[\mathbf{R}^m_{1,\mathrm{c}}(0;-\mu',\mu_0)] = L_\eta[\mathbf{R}^m_{\mathrm{g,c}}(-\mu',\mu_0)], \tag{51b}$$

$$L_\eta[\mathbf{R}^m_{1,\mathrm{s}}(0;-\mu,\mu')] = L_\eta[\mathbf{R}^m_{\mathrm{g,s}}(-\mu,\mu')], \tag{51c}$$

$$L_\eta[\mathbf{R}^m_{1,\mathrm{s}}(0;-\mu',\mu_0)] = L_\eta[\mathbf{R}^m_{\mathrm{g,s}}(-\mu',\mu_0)], \tag{51d}$$

$$L_\eta[\mathbf{R}^m_{2,\mathrm{c}}(0;-\mu,\mu_0)] = 0, \tag{51e}$$

$$L_\eta[\mathbf{R}^m_{p,\mathrm{s}}(0;-\mu,\mu_0)] = 0, \tag{51f}$$

$$L_\eta[\mathbf{R}_1(0;\mathbf{\Omega}_0)] = L_\eta[\mathbf{R}_{\mathrm{g}}(\mathbf{\Omega}_0)]. \tag{51g}$$

For a Lambertian surface, all the above derivatives would be identically zero except for the (1,1) elements of $L_\eta[\mathbf{R}^0_{1,\mathrm{c}}(0;-\mu,\mu')]$, $L_\eta[\mathbf{R}^0_{1,\mathrm{c}}(0;-\mu',\mu_0)]$ and $L_\eta[\mathbf{R}_1(0;\mathbf{\Omega}_0)]$ (these are equal to 1).

For the sun glint case (for which η is the wind speed W), we must first differentiate the Gaussian probability distribution of wave facet slopes and the shadow term in Eqs. (37) and (39) with respect to the mean square of the slopes s^2. Chain-rule differentiation using the empirical linear relation between and s^2 and W (Eq. (38)) furnishes the correct linearization.

5. The 2OS model: performance considerations and validation

A number of optimizations have been used to increase the speed and accuracy of the 2OS numerical RT code. Firstly, the Fourier coefficients of the phase matrix are computed using the expansion coefficients of the scattering matrix and generalized spherical functions [4]. This is much faster and more accurate than integrating over the azimuth. Secondly, we perform an exact first order of scattering using all the expansion coefficients; the second order of scattering then uses the Fourier coefficients computed with the first L+1 expansion coefficients, where L is the number of half-space quadrature streams. This technique substantially reduces the computational burden. Thirdly, quantities that do not depend on the Fourier component (such as $\Psi(\tau_{n+1};\mu^{-1}+\lambda_n)$) are calculated outside the Fourier loop. Fourthly, second-order calculations only require the Fourier coefficients of the phase matrix to be evaluated for four sets of directional cosines: $(-\mu,-\mu')$, $(-\mu,\mu')$, $(-\mu',\mu_0)$ and (μ',μ_0), where μ' indicates a quadrature value. This reduces the number of floating point operations by about $\frac{1}{2}L$. For unpolarized incident light (such as sunlight), Stokes parameters I and Q do not depend on the sine component of the second order reflection matrix $\mathbf{R}^m_{2,\mathrm{s}}$. Thus, $\mathbf{R}^m_{2,\mathrm{s}}$ is calculated only if U or V needs to be computed. Finally, special limiting cases (such as small layer optical thickness, zenith angles close to 0°, and zenith angles very close to each other or to quadrature angle values), are handled using appropriate Taylor series expansions.

To validate our code, we took the five-layer model from Kawabata and Ueno [7] and reproduced the Fourier coefficients of the reflection function due to the first two orders of scattering as shown in Table II of

that reference. The published results are in fact erroneous, and this was corroborated by the authors in a private communication. The new results using our method are presented in Table 1.

The results for all orders of scattering were obtained using a doubling-adding vector RT code [4]. The results produced with the expressions given in this paper are reasonable in view of the fact that the sum of the contributions from the first two orders of scattering become increasingly close to those for all orders of scattering as we go to the higher-order Fourier terms.

For the linearizations, all scalar intensity and reflection matrix analytic derivatives were validated by comparing them against derivative estimates using finite difference techniques. Further validation tests were carried out against a full vector model for the O_2 A band application; these are described in Section 6.

Table 1
Fourier coefficients of the reflection function for the 5-layer problem from Ref. [7]

m	All orders	1st + 2nd orders
0	1.16205(0)[a]	2.64969(−1)
1	−1.15467(−2)	−1.14072(−2)
2	6.78485(−4)	6.76188(−4)
3	−4.75188(−5)	−4.74920(−5)
4	5.88287(−6)	5.88180(−6)

[a]To be read as $1.16205 \times 10^{\circ}$.

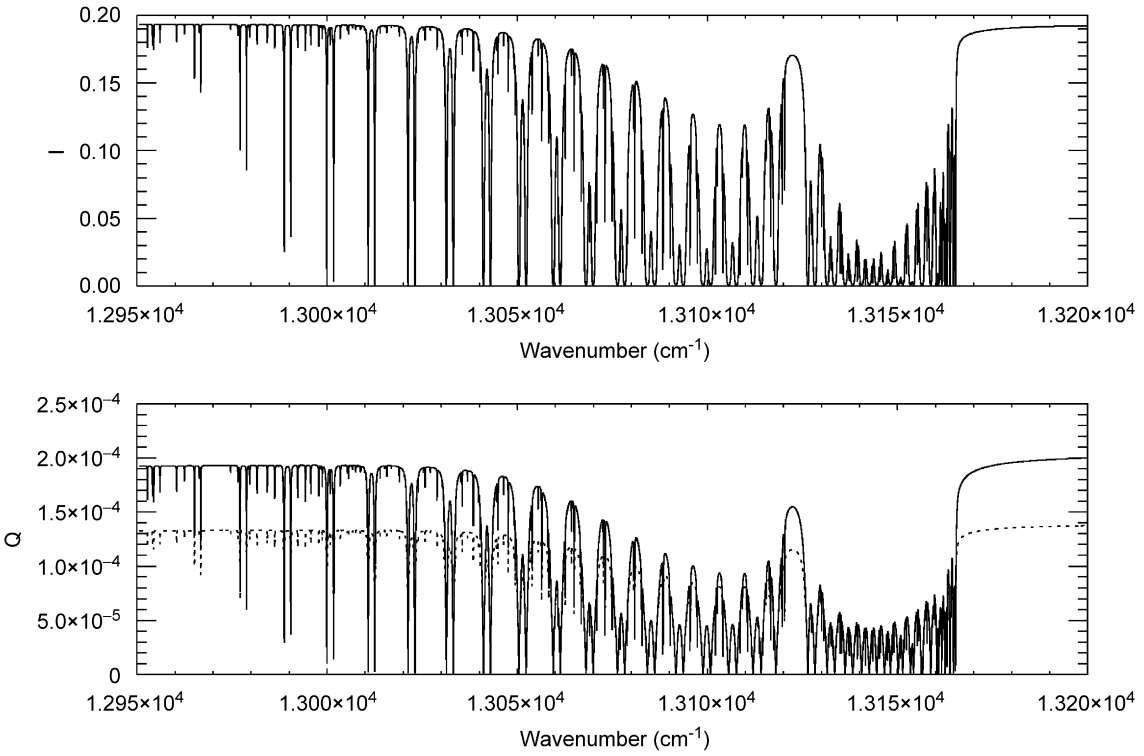

Fig. 1. Reflectance spectrum at the TOA in the O_2 A band. (Upper panel) Stokes parameter I; (Lower panel) Stokes parameter Q. The solid lines represent vector multiple scattering calculations. The dashed line for the Stokes parameter I is the sum of the intensity correction from the 2OS model and the scalar intensity. For the Stokes parameter Q, the dashed line represents the results from 2OS computations. The solar, viewing and relative azimuth angles are 50°, 30° and 60°,respectively.

6. Application to reflected sunlight measurements in the O_2 A band

The O_2 A band is used in remote sensing to retrieve surface pressure [19,20] and cloud top height [21–25]. We computed the intensity correction and Stokes parameter Q at the TOA for various geometries at gas absorption optical depths of 3.36×10^{-3}, 1.0 and 464.0 (representing the continuum, optical depth unity and center of a strong line, respectively). The aerosol extinction and Rayleigh scattering optical depths were 0.12 and 0.025, respectively. We used an 11-layer atmosphere, with the altitudes and level temperatures corresponding to the 1976 US Standard Model Atmosphere [26]. The atmosphere is bounded below by a Lambertian reflecting surface with albedo 0.3.

The gas absorption cross sections for the above calculations were computed assuming a Voigt line profile, with spectroscopic data taken from the HITRAN 2004 database [27]. A constant value of 0.2095 was used for the volume-mixing ratio of O_2. The Rayleigh scattering cross section was computed using the following standard equation [28]:

$$\sigma_r = \frac{24\pi^3}{\lambda^4 N^2} \frac{(n^2-1)^2}{(n^2+2)^2} \frac{6+3\rho}{6-7\rho}, \tag{52}$$

where σ_r, λ, N, n and ρ are, respectively, the Rayleigh scattering cross section per molecule, the wavelength (in microns), the molecular density, the refractive index and the depolarization factor (set to 0.0279 for air [29]).

The tropospheric aerosol was chosen to correspond to the climatological mixing group 4a of Kahn et al. [30], which is typical of much of North America. For the stratosphere (top 5 layers), a 75% solution of H_2SO_4 was assumed with a modified γ-size distribution [31]; the complex refractive index of the sulfuric acid solution was taken from the tables of Palmer and Williams [32]. Single scattering properties for the spherical-particle

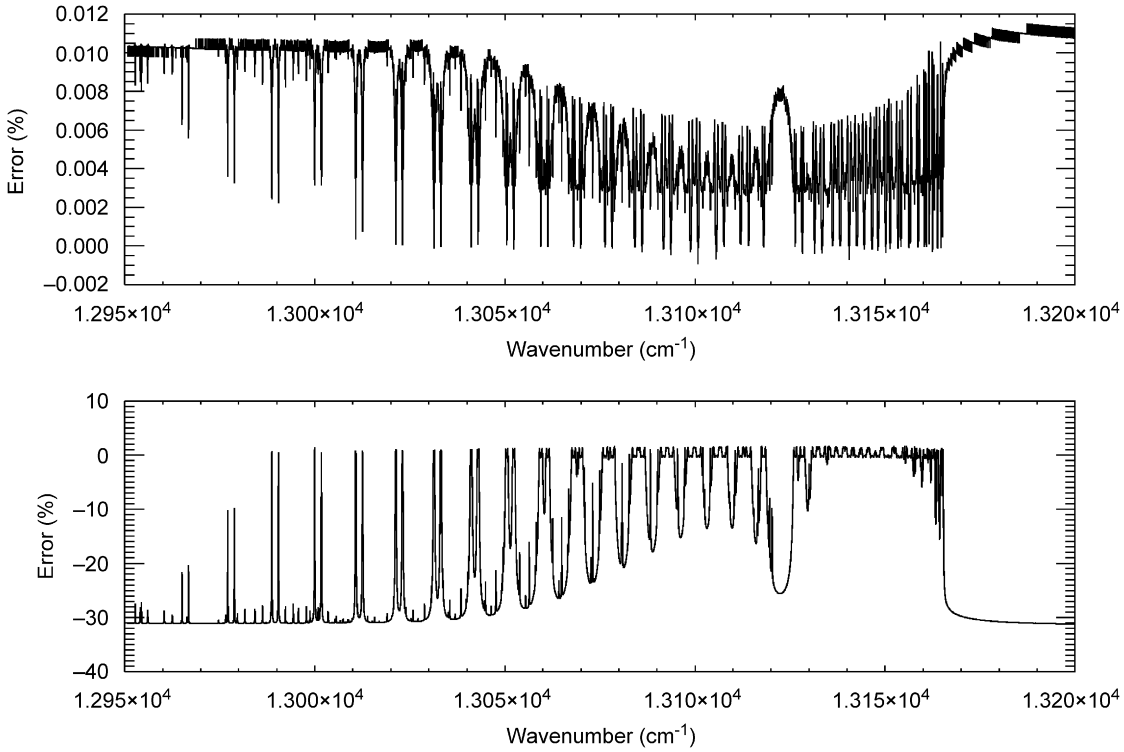

Fig. 2. Relative errors (%) using the 2OS model. (Upper panel) Stokes parameter I; (Lower panel) Stokes parameter Q. The error in the Stokes parameter I is the difference between the sum of the intensity correction from the 2OS model and the scalar intensity, and the intensity from a full vector multiple scattering calculation. The solar, viewing and relative azimuth angles are 50°, 30° and 60°,respectively.

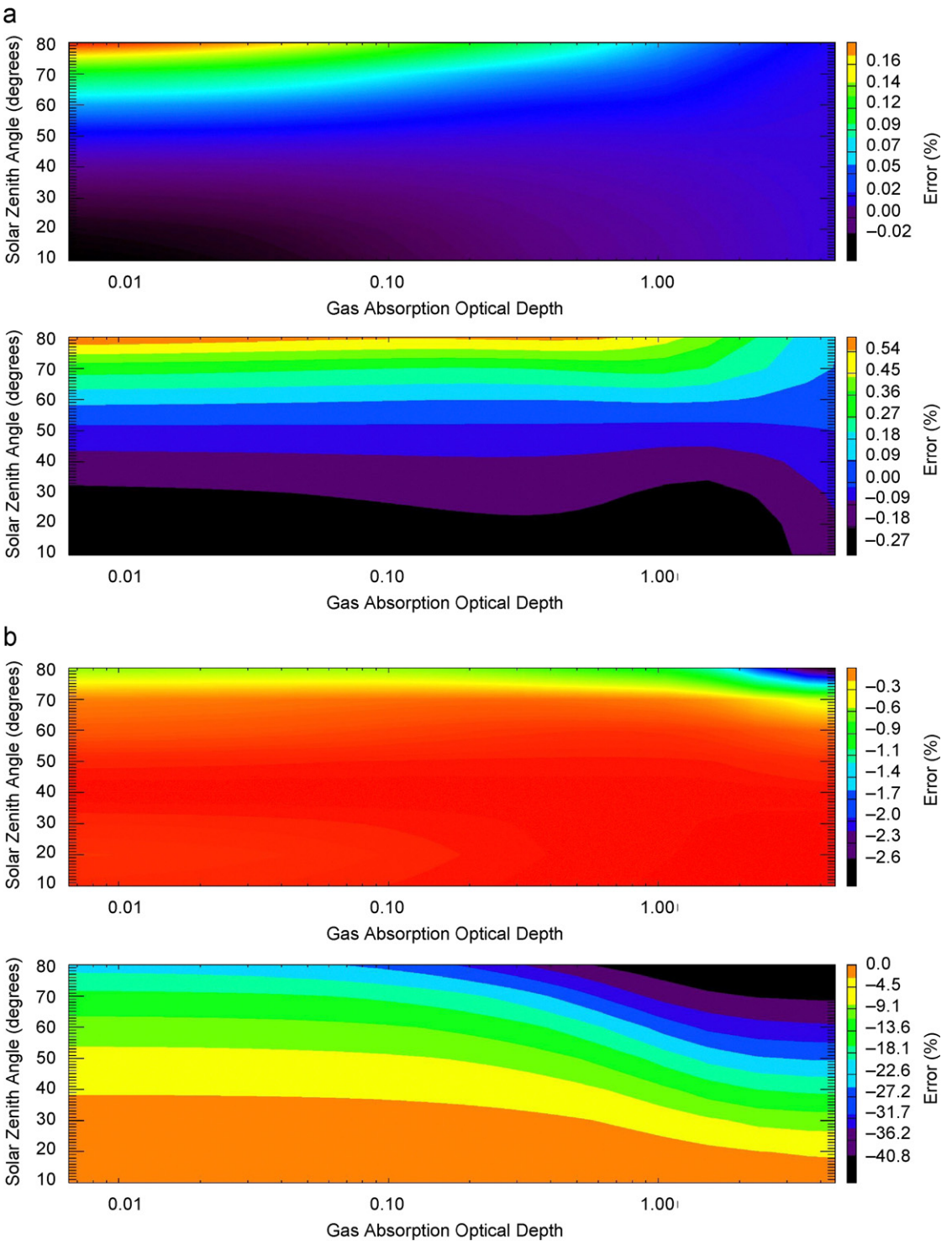

Fig. 3. (a) Errors in the intensity using the 2OS model (upper panel) and scalar model (lower panel) for nadir viewing scenario with surface albedo 0.05; (b) Errors in the polarized radiance for the same scenario.

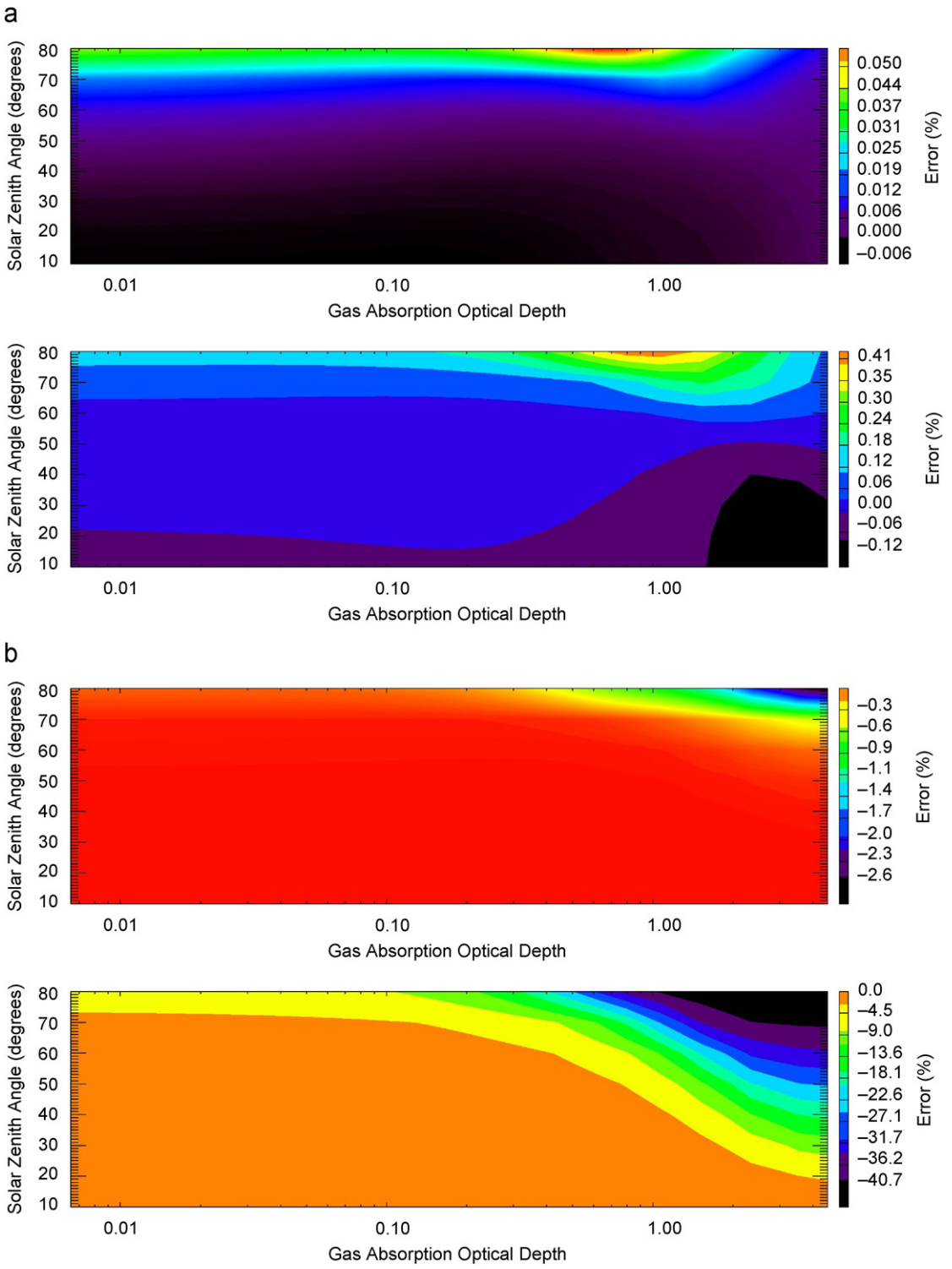

Fig. 4. Same as Fig. 3, except that the surface albedo is 0.5.

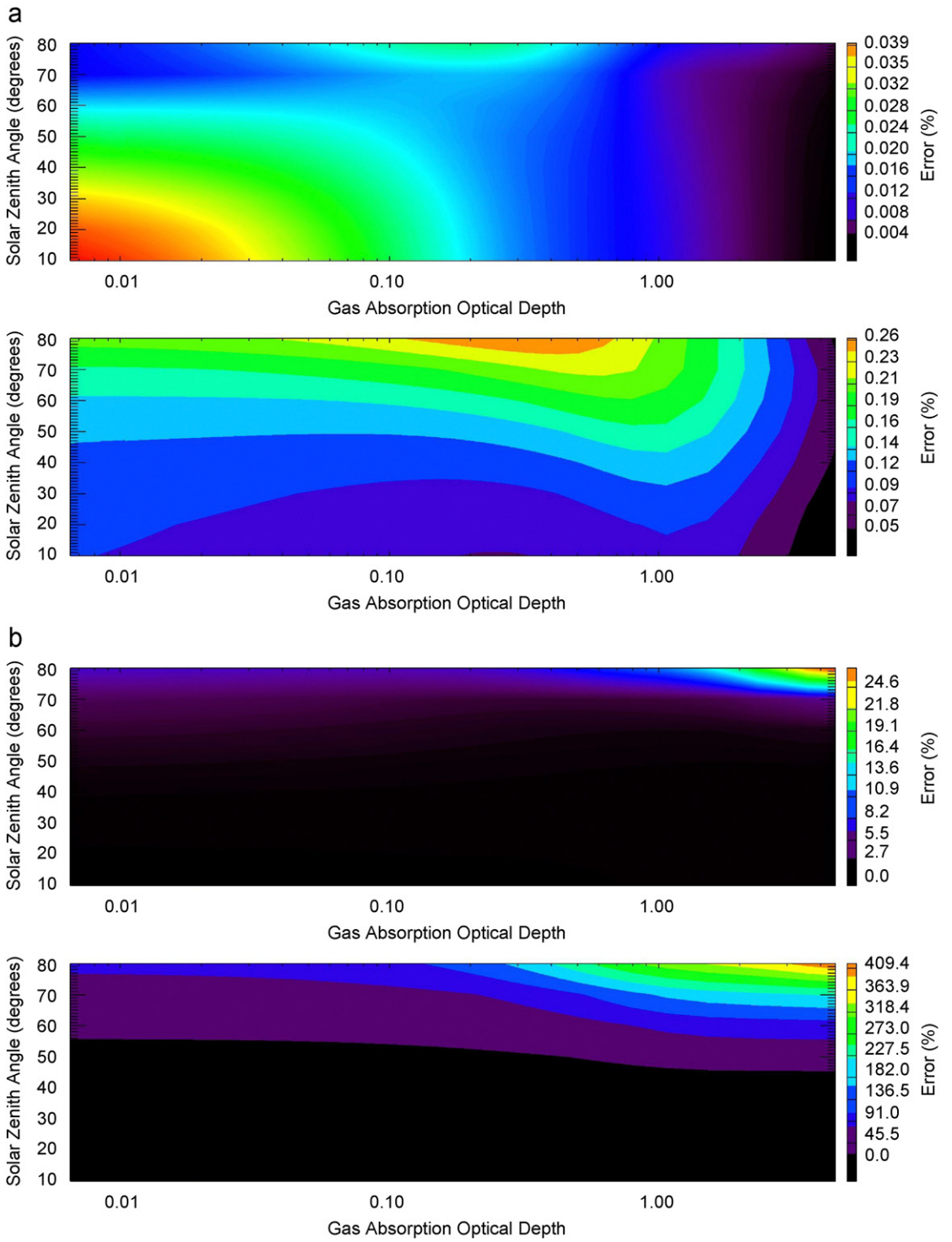

Fig. 5. Same as Fig. 3, except that the viewing angle is 60° and the azimuth angle 90°.

aerosols (such as sulfates and carbonaceous aerosols) were computed using a Mie scattering code [33] that generates coefficients for the expansion in generalized spherical functions. Accumulated and coarse dust properties were obtained using a T-matrix code [34]. A scale height of 1 km was assumed.

We compared our results with those obtained using a full multiple scattering discrete ordinate vector RT code [3]. Figs. 1 and 2 show, respectively, the reflectance spectrum and the error using the 2OS model. The solar, viewing and relative azimuth angles are 50°, 30° and 60°, respectively. The pseudo-spherical

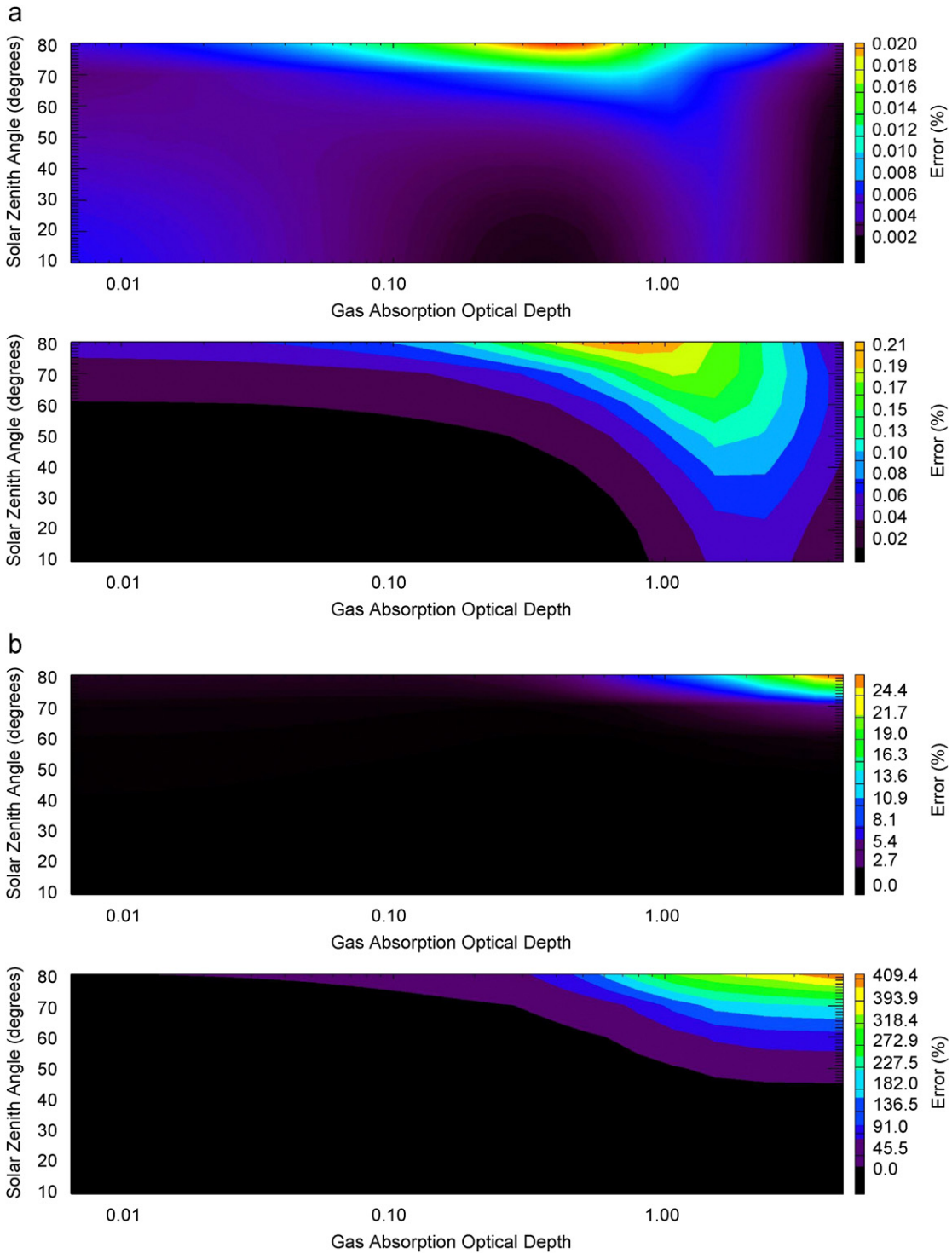

Fig. 6. Same as Fig. 5, except that the surface albedo is 0.5.

approximation was employed for the calculations. Clearly, the results using our model are exact in the line cores and most inaccurate (~30% error in the Stokes parameter Q) in the continuum. However, the continuum is a region dominated by multiple scattering and polarization is least significant there. This suggests that, while the 2OS model may not always provide Stokes parameter Q with sufficiently high accuracy, the polarization ($-Q/I$), or one of its orthogonal components ($I \pm Q$), can be obtained very accurately.

We tested this hypothesis for various solar zenith angles from 10° to 80°, viewing angles 0° and 60°, azimuth angles 0° and 90° and surface albedos 0.05 and 0.5. Figs. 3(a) and (b) show the errors in the intensity and the component of radiance polarized perpendicular to the principal plane, $(I-Q)/2$ (hereafter referred to as the polarized radiance), for nadir viewing and surface albedo 0.05. The upper panels in these plots show the errors using the 2OS model, while the lower panels show errors using the scalar approximation. As the solar zenith angle increases, the scattering angle increases; hence the polarization increases and the errors are larger. Also, at small solar zenith angles, the errors in the polarized radiance (using the 2OS model) go from larger in regions of small gas absorption (continuum) to smaller in regions of high gas absorption (line cores). This is because in the continuum there is multiple scattering while in the line cores the atmosphere is opaque and what we see is primarily single scattering in the upper atmosphere. However, the reverse behavior is seen at very high solar zenith angles. Here, the high scattering angle contributes to increased scattering in the line cores, while increased attenuation of the solar beam decreases the contribution from the surface in the continuum.

Figs. 4–6 show the same errors for different viewing geometries and surface albedos. It is clear that higher surface albedos give rise to smaller errors. An interesting feature for non-nadir viewing geometries is that we need to consider rotation angles (to transform from the solar and viewing planes to the scattering plane). The

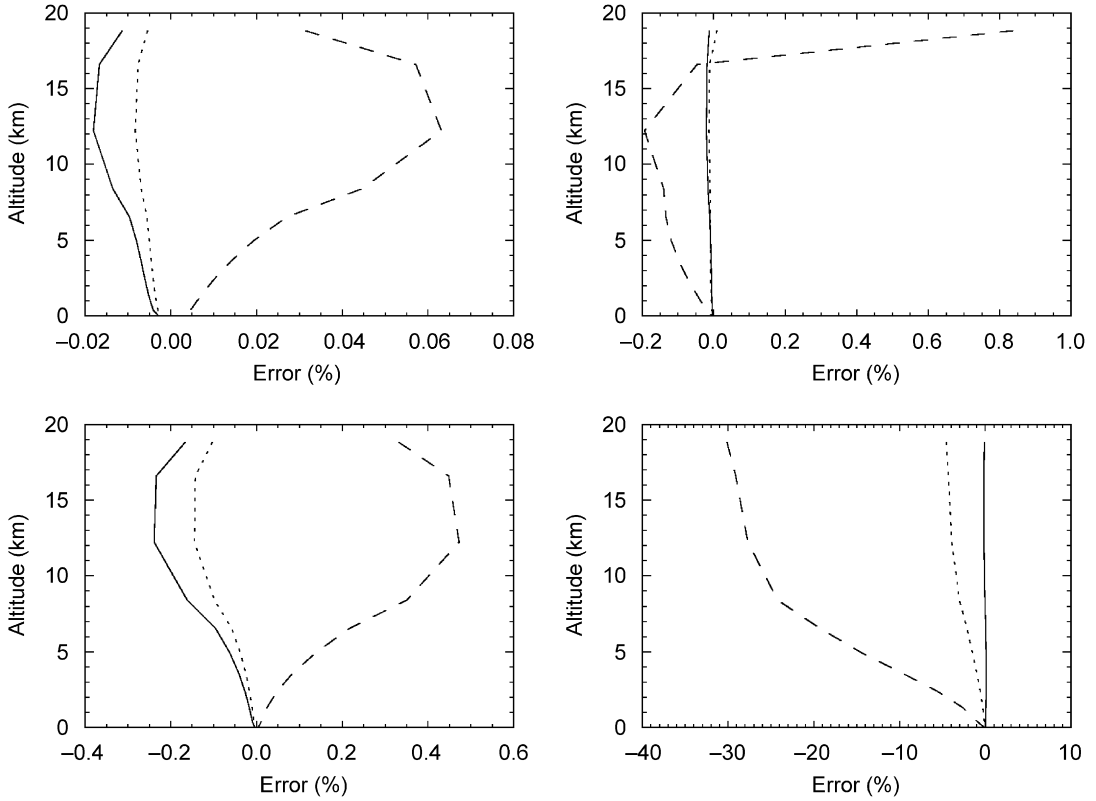

Fig. 7. Errors in the weighting functions with respect to gas absorption optical depth for the intensity using the 2OS (upper left panel) and scalar (upper right panel) models and the polarized radiance using the same models (lower panels). The solid, dotted and dashed lines refer to solar zenith angles of 10°, 40° and 70°,respectively. The gas absorption optical depth is 1.07.

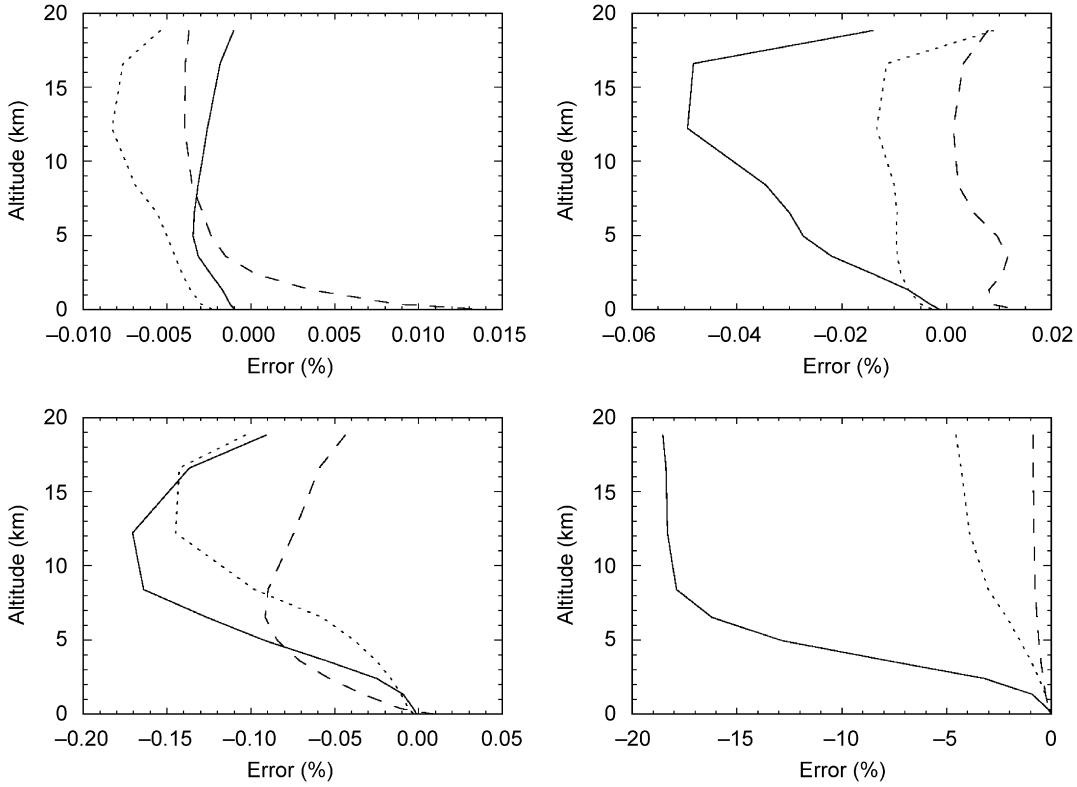

Fig. 8. Same as Fig. 7, except that the solar zenith angle is 40°. The solid, dotted and dashed lines refer to gas absorption optical depths of 4.55, 1.07 and 0.01, respectively.

rotation angles go from below 90° at low solar zenith angles to above 90° at high solar zenith angles, causing a reversal in the sign of polarization; the radiation goes from being predominantly *s*-polarized to *p*-polarized. The improvement using the 2OS model is evident in all the plots, especially for the polarized radiance, where there is an order of magnitude reduction in the errors.

The accuracy of the weighting functions with respect to gas absorption optical depth was investigated for several solar zenith angles (Fig. 7) and optical depths (Fig. 8). The surface albedo was assumed to be 0.3 and nadir-viewing geometry was employed. In Fig. 7, the solid, dotted and dashed lines refer to solar zenith angles 10°, 40° and 70°, respectively. In Fig. 8, they denote gas absorption optical depths 4.55, 1.07 and 0.01, respectively. From upper left to lower right, the different panels represent errors in the weighting functions for the intensity using the 2OS and scalar models and polarized radiance using the same models. Clearly, the 2OS model gives an order of magnitude (or more) reduction in the errors.

Similar tests were done for ocean glint scenarios using two wind speeds (4 m/s in Fig. 9 and 8 m/s in Fig. 10). The difference between this case and the Lambertian one is that the ocean surface is highly polarizing. In some cases, the polarization due to the surface can be higher than that due to atmospheric scattering (see, *e.g.* lower panels in Figs. 3(b) and 9(b)). Increasing wind speed is analogous to decreasing surface albedo; errors are thus larger at higher wind speeds. Figs. 11 show the weighting functions for the intensity (upper panels) and polarized radiance (lower panels) with respect to the wind speed. The gas absorption optical depth is 0.01, 1.07 and 4.55 in Figs. 11(a), (b) and (c), respectively. The 2OS model gives results very close to those from a full vector multiple scattering calculation.

Finally, the effect of sphericity was investigated by increasing the solar zenith angle close to 90° Figs. 12(a) and (b) show the errors in the intensity and polarized radiance for nadir viewing and surface albedo 0.3. The upper panel in these plots shows the errors using the 2OS model and the lower panel shows the errors using the scalar approximation. The 2OS model gives excellent results up to a solar zenith angle of about 80°.

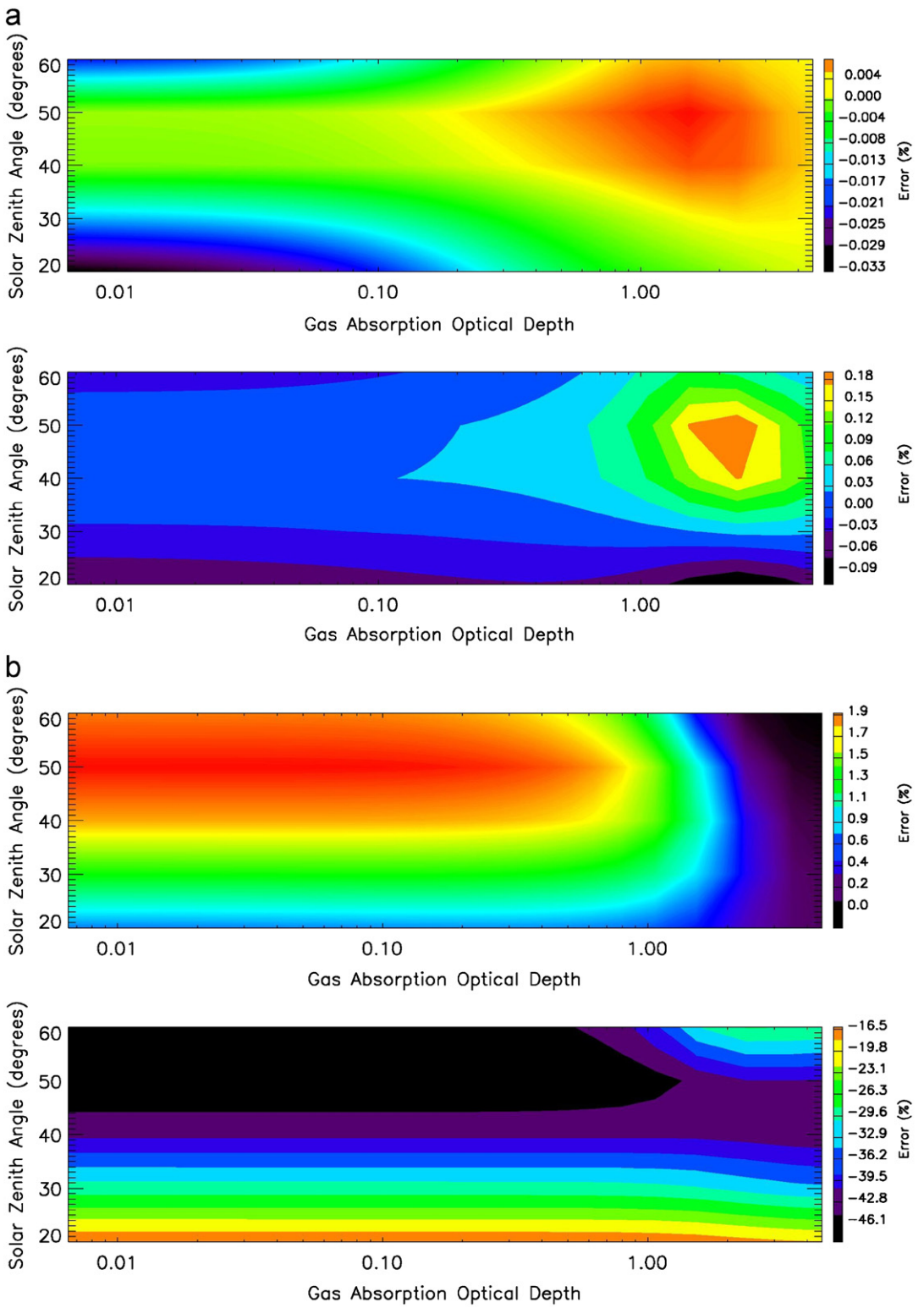

Fig. 9. Same as Fig. 3, bur with results for an ocean sun glint scenario with wind speed of 4 m/s.

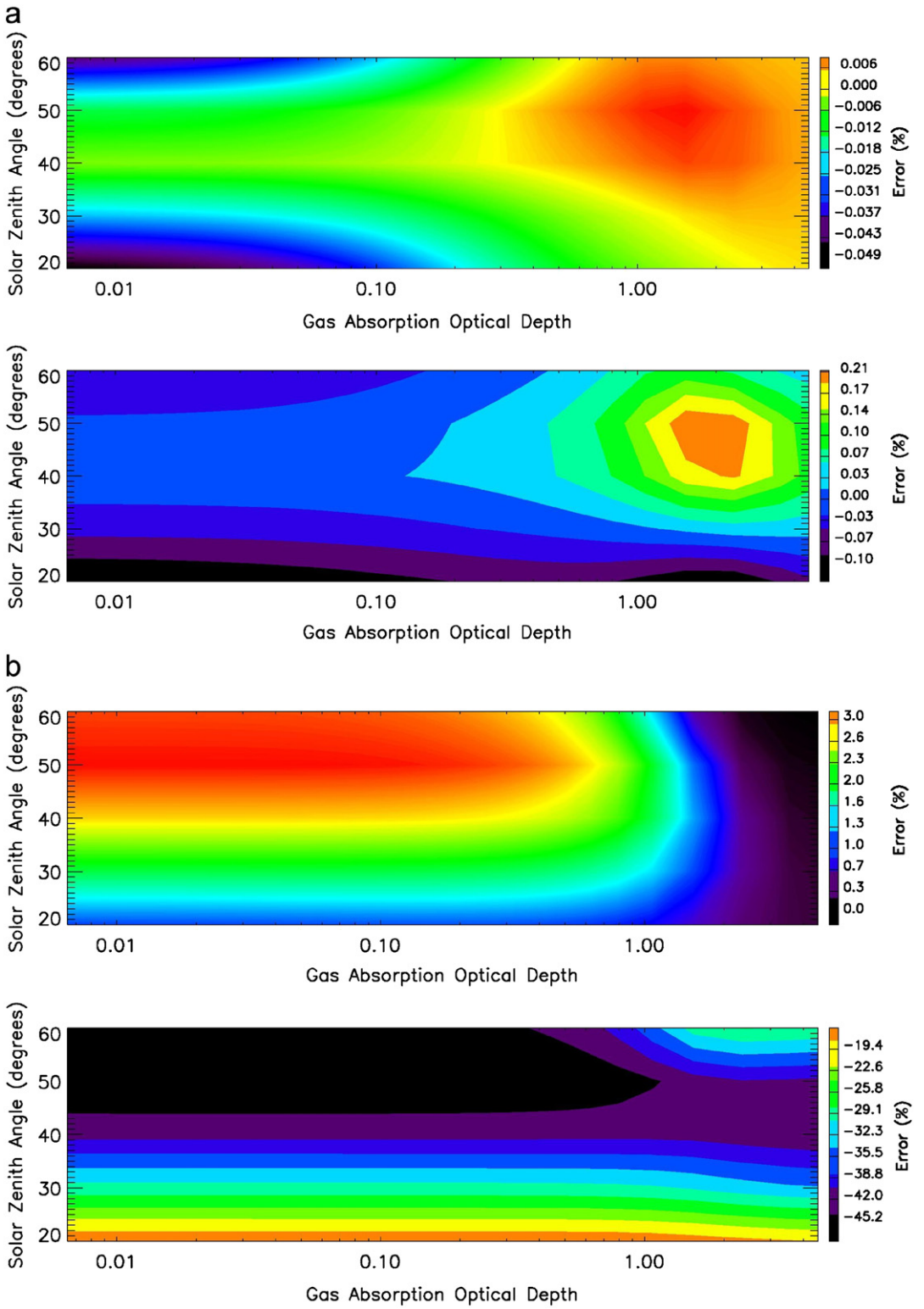

Fig. 10. Same as Fig. 9, except that the wind speed is 8 m/s.

7. Concluding remarks

We have developed a polarized RT model to calculate the reflection matrix for the first two orders of scattering in vertically inhomogeneous, scattering-absorbing media. Solar beam attenuation has been treated for a curved spherical-shell atmosphere. In addition, the model computes a scalar–vector intensity correction induced by polarization. This correction is intended for use in conjunction with the results from a scalar multiple scattering calculation to approximate the full Stokes-vector intensity with polarization included. We have also performed a complete analytic differentiation (linearization) of the RT equations, allowing the model to deliver weighting functions with respect to any atmospheric or surface parameters.

Intensity results have been compared with those from Kawabata and Ueno [7] for scalar intensity, and against vector output from Hovenier [6] for a homogeneous plane–parallel atmosphere. We have also performed backscatter simulations of reflected sunlight in the O_2 A band for a variety of geometries, and compared our results with those from a full vector multiple scattering code [3]. The effects of gas absorption optical depth, solar zenith angle, viewing geometry, surface albedo and wind speed (in the case of ocean glint) on the intensity, polarized radiance and respective weighting functions have been investigated. In all cases, the 2OS model provides a reliable and accurate correction to the intensity field and associated weighting function derivatives.

It is worth noting that the 2OS computation is two orders of magnitude faster than a full vector calculation and adds only about 10% CPU overhead to a multiple scattering scalar intensity calculation. This consideration is important for operational retrievals based on *ab initio* forward model RT simulations. It can enable accurate polarized-light simulations to be made without the use of a prohibitively slow full Stokes vector computation, or the use of an intensity correction look-up table.

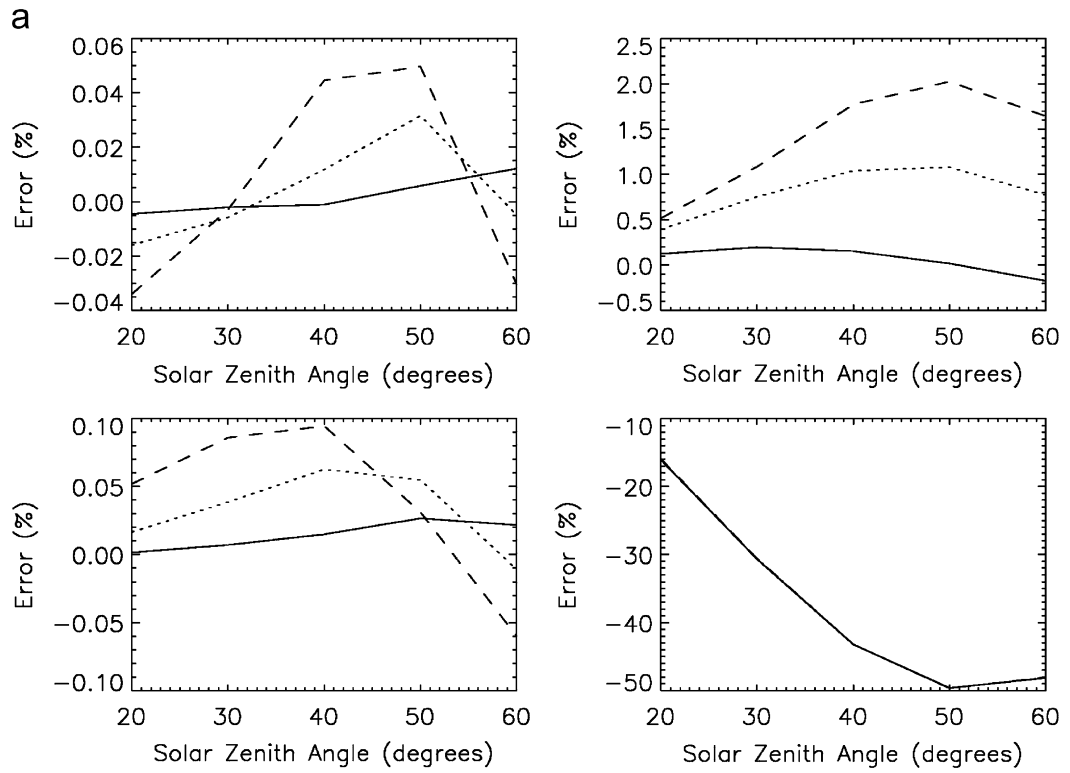

Fig. 11. Errors in the weighting functions with respect to wind speed for the intensity using the 2OS (upper left panel) and scalar (upper right panel) models and the polarized radiance using the same models (lower panels). The solid, dotted and dashed lines refer to wind speeds of 4, 8 and 12 m/s, respectively. The gas absorption optical depth is 0.01, 1.07 and 4.55 in plots (a), (b) and (c), respectively.

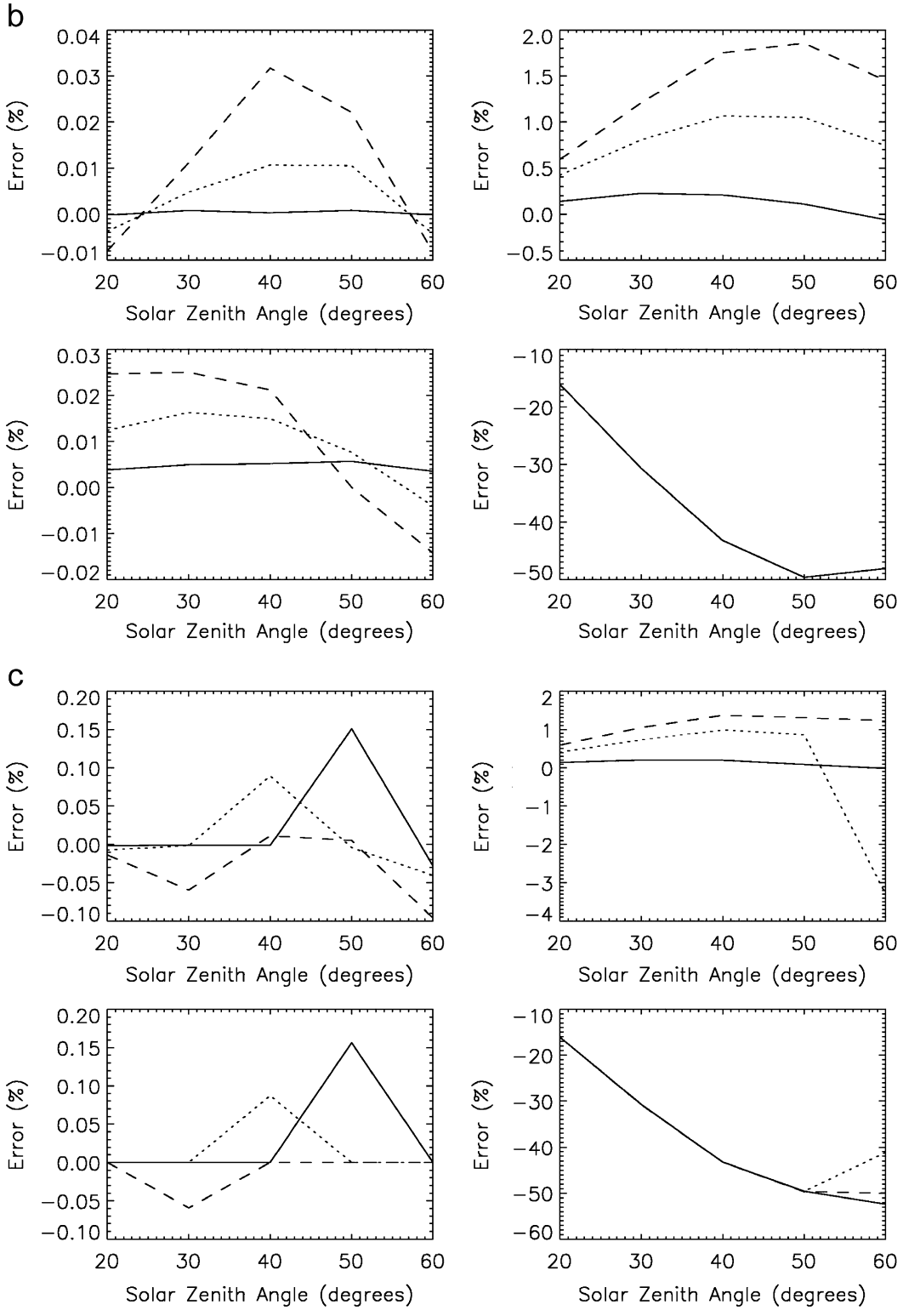

Fig. 11. (*Continued*)

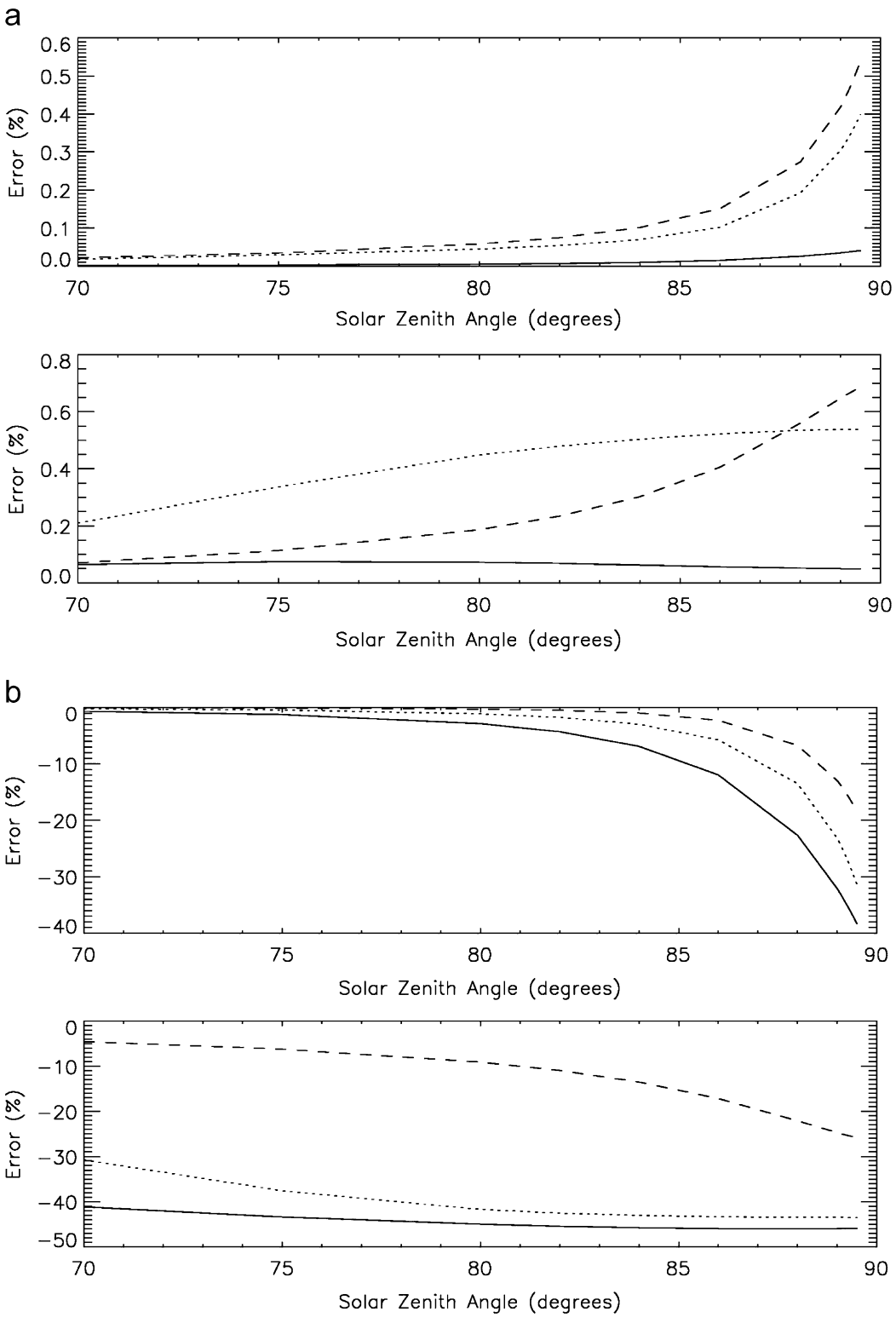

Fig. 12. Same as Fig. 3, except that the surface albedo is 0.3. The effect of sphericity is being tested here.

Acknowledgments

The research described in this paper was performed for the Orbiting Carbon Observatory Project at the Jet Propulsion Laboratory, California Institute of Technology, under contracts with the National Aeronautics and Space Administration. This work was supported in part by NASA Grant NAG1-1806.

The authors would like to thank Yuk Yung for his support and generous assistance; Joop Hovenier and Johan de Haan for providing us with a doubling-adding vector RT code to validate our model; and Run-Lie Shia for valuable suggestions to improve the manuscript.

Appendix A

Linearization of the second-order contributions to the reflection matrices follows the principles laid down in Section 4.

We consider the cosine contributions first. Eq. (29a) can be rewritten as:

$$\begin{aligned}\mathbf{R}^m_{2,\mathrm{c}}(L_{n+1};-\mu,\mu_0) = \mathbf{R}^m_{2,\mathrm{c}}(L_n;-\mu,\mu_0)Q_n(\mu,\lambda_n) &+ \frac{\omega_n}{2\mu}\int_0^1 \mathbf{P}^m_{\mathrm{c}}(-\mu,-\mu')\mathbf{V}^m_1(-\mu',\mu_0)\,\mathrm{d}\mu' \\ &+ \frac{\omega_n}{2\mu}\int_0^1 \mathbf{P}^m_{\mathrm{s}}(-\mu,-\mu')\mathbf{V}^m_2(-\mu',\mu_0)\,\mathrm{d}\mu' \\ &+ \frac{\omega_n\lambda_n}{2}\int_0^1 \mathbf{V}^m_3(-\mu,\mu')\mathbf{P}^m_{\mathrm{c}}(\mu',\mu_0)\,\mathrm{d}\mu' - \frac{\omega_n\lambda_n}{2}\int_0^1 \mathbf{V}^m_4(-\mu,\mu')\mathbf{P}^m_{\mathrm{s}}(\mu',\mu_0)\,\mathrm{d}\mu'. \end{aligned} \tag{A.1}$$

The Fourier components of the phase matrices can be expressed in terms of input expansion coefficients $\mathbf{B}_{nl}$ (*cf*. Eqs. (20)), so their linearizations will be known functions of the coefficient derivatives $\mathbf{z}_{nl}$. We express this as follows:

$$L_k[\mathbf{P}^m_{\mathrm{c}}] = g^m(\mathbf{z}_{nl})\delta_{nk} \equiv \mathbf{G}^m_{nk}, \tag{A.2a}$$

$$L_k[\mathbf{P}^m_{\mathrm{s}}] = j^m(\mathbf{z}_{nl})\delta_{nk} \equiv \mathbf{J}^m_{nk}. \tag{A.2b}$$

Now we differentiate Eq. (A.1) to yield:

$$\begin{aligned} L_k[\mathbf{R}^m_{2,\mathrm{c}}(L_{n+1};-\mu,\mu_0)] = L_k[\mathbf{R}^m_{2,\mathrm{c}}(L_n;-\mu,\mu_0)]Q_n(\mu,\lambda_n) &+ \mathbf{R}^m_{2,\mathrm{c}}(L_n;-\mu,\mu_0)H_{nk}(\mu,\lambda_n) \\ &+ \frac{1}{2\mu}\int_0^1 \mathbf{V}^m_1(-\mu',\mu_0)[\omega_n\mathbf{G}^m_{nk}(-\mu,-\mu') + u_n\delta_{nk}\mathbf{P}^m_{\mathrm{c}}(-\mu,-\mu')]\,\mathrm{d}\mu' \\ &+ \frac{1}{2\mu}\int_0^1 \mathbf{W}^m_{1,nk}(-\mu',\mu_0)\omega_n\mathbf{P}^m_{\mathrm{c}}(-\mu,-\mu')\,\mathrm{d}\mu' \\ &+ \frac{\lambda_n}{2}\int_0^1 \mathbf{V}^m_3(-\mu,\mu')[\omega_n\mathbf{G}^m_{nk}(\mu',\mu_0) + u_n\delta_{nk}\mathbf{P}^m_{\mathrm{c}}(\mu',\mu_0)]\,\mathrm{d}\mu' \\ &+ \frac{\lambda_n}{2}\int_0^1 \mathbf{W}^m_{3,nk}(-\mu,\mu')\omega_n\mathbf{P}^m_{\mathrm{c}}(\mu',\mu_0)\,\mathrm{d}\mu' + \frac{\omega_n\sigma_{nk}}{2}\int_0^1 \mathbf{V}^m_3(-\mu,\mu')\mathbf{P}^m_{\mathrm{c}}(\mu',\mu_0)\,\mathrm{d}\mu' \\ &+ \frac{1}{2\mu}\int_0^1 \mathbf{V}^m_2(-\mu',\mu_0)[\omega_n\mathbf{J}^m_{nk}(-\mu,-\mu') + u_n\delta_{nk}\mathbf{P}^m_{\mathrm{s}}(-\mu,-\mu')]\,\mathrm{d}\mu' \\ &+ \frac{1}{2\mu}\int_0^1 \mathbf{W}^m_{2,nk}(-\mu',\mu_0)\omega_n\mathbf{P}^m_{\mathrm{s}}(-\mu,-\mu')\,\mathrm{d}\mu' \\ &- \frac{\lambda_n}{2}\int_0^1 \mathbf{V}^m_4(-\mu,\mu')[\omega_n\mathbf{J}^m_{nk}(\mu',\mu_0) + u_n\delta_{nk}\mathbf{P}^m_{s}(\mu',\mu_0)]\,\mathrm{d}\mu' \\ &- \frac{\lambda_n}{2}\int_0^1 \mathbf{W}^m_{4,nk}(-\mu,\mu')\omega_n\mathbf{P}^m_{\mathrm{s}}(\mu',\mu_0)\,\mathrm{d}\mu' - \frac{\omega_n\sigma_{nk}}{2}\int_0^1 \mathbf{V}^m_4(-\mu,\mu')\mathbf{P}^m_{\mathrm{s}}(\mu',\mu_0)\,\mathrm{d}\mu'. \end{aligned} \tag{A.3}$$

The only new quantities to be determined are the linearizations:

$$\mathbf{W}^m_{1,nk} \equiv L_k[\mathbf{V}^m_1], \tag{A.4a}$$

$$\mathbf{W}^m_{2,nk} \equiv L_k[\mathbf{V}^m_2], \tag{A.4b}$$

$$\mathbf{W}^m_{3,nk} \equiv L_k[\mathbf{V}^m_3], \tag{A.4c}$$

$$\mathbf{W}^m_{4,nk} \equiv L_k[\mathbf{V}^m_4]. \tag{A.4d}$$

We evaluate the following quantities first:

$$L_k[Q_n(\mu', \lambda_n)] = -Q_n(\mu', \lambda_n)[(x' + \lambda_n)v_n\delta_{nk} + \Delta_n\sigma_{nk}] \equiv H_{nk}(\mu', \lambda_n), \tag{A.5a}$$

$$L_k[Q_n(\mu, \lambda_n)] = -Q_n(\mu, \lambda_n)[(\mu^{-1} + \lambda_n)v_n\delta_{nk} + \Delta_n\sigma_{nk}] \equiv H_{nk}(\mu, \lambda_n), \tag{A.5b}$$

$$L_k[Q_n(\mu, x')] = -Q_n(\mu, x')[(\mu^{-1} + x')v_n\delta_{nk}] \equiv H_{nk}(\mu, x'). \tag{A.5c}$$

From Eqs. (24), (43a) and (A.5), we derive the following:

$$\begin{aligned} &L_k[\Phi(L_{n+1}; \mu^{-1}, x', \lambda_n)] \\ &\quad = \left\{ \begin{array}{ll} \frac{H_{nk}(\mu,\lambda_n) - H_{nk}(\mu',\lambda_n)}{x' - \mu^{-1}}, & x' \neq \mu^{-1} \\ (\tau_{n+1} - \tau_n)H_{nk}(\mu, \lambda_n), & x' = \mu^{-1} \end{array} \right\}, \\ &\quad \equiv \Gamma^1_{nk}(\mu^{-1}, x', \lambda_n) \end{aligned} \tag{A.6a}$$

$$\begin{aligned} &L_k[\Phi(L_{n+1}; x', \lambda_n, \mu^{-1})] \\ &\quad = \left\{ \begin{array}{ll} \frac{H_{nk}(\mu,x') - H_{nk}(\mu,\lambda_n)}{\lambda_n - x'} - \frac{\sigma_{nk}\Phi(L_{n+1};x',\lambda_n,\mu^{-1})}{\lambda_n - x'}, & x' \neq \lambda_n \\ (\tau_{n+1} - \tau_n)H_{nk}(\mu, \lambda_n), & x' = \lambda_n \end{array} \right\}. \\ &\quad \equiv \Gamma^2_{nk}(x', \lambda_n, \mu^{-1}) \end{aligned} \tag{A.6b}$$

Further, we note that:

$$L_k[E_n(\mu, x')] = -\frac{\mu^{-1}x'H_{nk}(\mu, x')}{4(\mu^{-1} + x')} \equiv F_{nk}(\mu, x'), \tag{A.7a}$$

$$\begin{aligned} L_k[E_n(\mu', \lambda_n)] &= \left(\frac{x'\sigma_{nk}}{4(x' + \lambda_n)} - \frac{x'\lambda_n\sigma_{nk}}{4(x' + \lambda_n)^2}\right)\left(1 - Q_n(\mu', \lambda_n)\right) - \frac{x'\lambda_n H_{nk}(\mu', \lambda_n)}{4(x' + \lambda_n)} \\ &= \frac{(x')^2\sigma_{nk}(1 - Q_n(\mu', \lambda_n))}{4(x' + \lambda_n)^2} - \frac{x'\lambda_n H_{nk}(\mu', \lambda_n)}{4(x' + \lambda_n)} \equiv F_{nk}(\mu', \lambda_n). \end{aligned} \tag{A.7b}$$

Eqs. (26) and (27) can now be differentiated to obtain:

$$\begin{aligned} L_k[\mathbf{R}^m_{1,c}(L_{n+1}; -\mu, \mu')] = {} & L_k[\mathbf{R}^m_{1,c}(L_n; -\mu, \mu')]Q_n(\mu, x') \\ & + \mathbf{R}^m_{1,c}(L_n; -\mu, \mu')H_{nk}(\mu, x') + \omega_n E_n(\mu, x')\mathbf{G}^m_{nk}(-\mu, \mu') \\ & + \mathbf{P}^m_c(-\mu, \mu')[F_{nk}(\mu, x')\omega_n + E_n(\mu, x')u_n\delta_{nk}] \equiv \mathbf{S}^m_{3,nk}, \end{aligned} \tag{A.8a}$$

$$\begin{aligned} L_k[\mathbf{R}^m_{1,c}(L_{n+1}; -\mu', \mu_0)] = {} & L_k[\mathbf{R}^m_{1,c}(L_n; -\mu', \mu_0)]Q_n(\mu', \lambda_n) \\ & + \mathbf{R}^m_{1,c}(L_n; -\mu', \mu_0)H_{nk}(\mu', \lambda_n) + \omega_n E_n(\mu', \lambda_n)\mathbf{G}^m_{nk}(-\mu', \mu_0) \\ & + \mathbf{P}^m_c(-\mu', \mu_0)[F_{nk}(\mu', \lambda_n)\omega_n + E_n(\mu', \lambda_n)u_n\delta_{nk}] \equiv \mathbf{S}^m_{1,nk}, \end{aligned} \tag{A.8b}$$

$$L_k[\mathbf{R}^m_{1,\mathrm{s}}(L_{n+1};-\mu,\mu')] = L_k[\mathbf{R}^m_{1,\mathrm{s}}(L_n;-\mu,\mu')]Q_n(\mu,x') + \mathbf{R}^m_{1,\mathrm{s}}(L_n;-\mu,\mu')H_{nk}(\mu,x') + \omega_n E_n(\mu,x')\mathbf{J}^m_{nk}(-\mu,\mu') + \mathbf{P}^m_{\mathrm{s}}(-\mu,\mu')[F_{nk}(\mu,x)'\omega_n + E_n(\mu,x')u_n\delta_{nk}] \equiv \mathbf{S}^m_{4,nk}, \tag{A.8c}$$

$$L_k[\mathbf{R}^m_{1,\mathrm{s}}(L_{n+1};-\mu',\mu_0)] = L_k[\mathbf{R}^m_{1,\mathrm{s}}(L_n;-\mu',\mu_0)]Q_n(\mu',\lambda_n) + \mathbf{R}^m_{1,\mathrm{s}}(L_n;-\mu',\mu_0)H_{nk}(\mu',\lambda_n) + \omega_n E_n(\mu',\lambda_n)\mathbf{J}^m_{nk}(-\mu',\mu_0). + \mathbf{P}^m_{\mathrm{s}}(-\mu',\mu_0)[F_{nk}(\mu',\lambda_n)\omega_n + E_n(\mu',\lambda_n)u_n\delta_{nk}] \equiv \mathbf{S}^m_{2,nk}. \tag{A.8d}$$

The above expressions can be used to evaluate the quantities in Eqs. (A.4):

$$\mathbf{W}^m_{1,nk}(-\mu',\mu_0) = \Gamma^1_{nk}(\mu^{-1},x',\lambda_n)\mathbf{R}^m_{1,\mathrm{c}}(L_n;-\mu',\mu_0) + \mathbf{S}^m_{1,nk}\Phi(L_{n+1};\mu^{-1},x',\lambda_n) + \left\{\mathbf{G}^m_{nk}(-\mu',\mu_0)\omega_n + \mathbf{P}^m_{\mathrm{c}}(-\mu',\mu_0)u_n\delta_{nk}\right\}\left\{\frac{x'}{\mu^{-1}}\frac{E_n(\mu,\lambda_n)}{x'+\lambda_n} - \frac{x'\lambda_n}{4(x'+\lambda_n)}\Phi(L_{n+1};\mu^{-1},x',\lambda_n)\right\} + \mathbf{P}^m_{\mathrm{c}}(-\mu',\mu_0)\omega_n\left\{\begin{array}{l}\frac{x'}{\mu^{-1}}\frac{F_{nk}(\mu,\lambda_n)}{x'+\lambda_n} - \frac{x'}{\mu^{-1}}\frac{E_n(\mu,\lambda_n)\sigma_{nk}}{(x'+\lambda_n)^2} - \frac{x'\sigma_{nk}}{4(x'+\lambda_n)}\Phi(L_{n+1};\mu^{-1},x',\lambda_n)\\ +\frac{x'\lambda_n\sigma_{nk}}{4(x'+\lambda_n)^2}\Phi(L_{n+1};\mu^{-1},x',\lambda_n) - \frac{x'\lambda_n}{4(x'+\lambda_n)}\Gamma^1_{nk}(\mu^{-1},x',\lambda_n)\end{array}\right\}, \tag{A.9a}$$

$$\mathbf{W}^m_{2,nk}(-\mu',\mu_0) = \Gamma^1_{nk}(\mu^{-1},x',\lambda_n)\mathbf{R}^m_{1,\mathrm{s}}(L_n;-\mu',\mu_0) + \mathbf{S}^m_{2,nk}\Phi(L_{n+1};\mu^{-1},x',\lambda_n) + \left\{\boldsymbol{J}^m_{nk}(-\mu',\mu_0)\omega_n + \mathbf{P}^m_{\mathrm{s}}(-\mu',\mu_0)u_n\delta_{nk}\right\}\left\{\frac{x'}{\mu^{-1}}\frac{E_n(\mu,\lambda_n)}{x'+\lambda_n} - \frac{x'\lambda_n}{4(x'+\lambda_n)}\Phi(L_{n+1};\mu^{-1},x',\lambda_n)\right\} + \boldsymbol{P}^m_{\mathrm{s}}(-\mu',\mu_0)\omega_n\left\{\begin{array}{l}\frac{x'}{\mu^{-1}}\frac{F_{nk}(\mu,\lambda_n)}{x'+\lambda_n} - \frac{x'}{\mu^{-1}}\frac{E_n(\mu,\lambda_n)\sigma_{nk}}{(x'+\lambda_n)^2} - \frac{x'\sigma_{nk}}{4(x'+\lambda_n)}\Phi(L_{n+1};\mu^{-1},x',\lambda_n)\\ +\frac{x'\lambda_n\sigma_{nk}}{4(x'+\lambda_n)^2}\Phi(L_{n+1};\mu^{-1},x',\lambda_n) - \frac{x'\lambda_n}{4(x'+\lambda_n)}\Gamma^1_{nk}(\mu^{-1},x',\lambda_n)\end{array}\right\}, \tag{A.9b}$$

$$\mathbf{W}^m_{3,nk}(-\mu,\mu') = \Gamma^2_{nk}(x',\lambda_n,\mu^{-1})\mathbf{R}^m_{1,\mathrm{c}}(L_n;-\mu,\mu') + \mathbf{S}^m_{3,nk}\Phi(L_{n+1};x',\lambda_n,\mu^{-1}) + \left\{\mathbf{G}^m_{nk}(-\mu,\mu')\omega_n + \mathbf{P}^m_{\mathrm{c}}(-\mu,\mu')u_n\delta_{nk}\right\}\left\{\frac{x'}{\lambda_n}\frac{E_n(\mu,\lambda_n)}{x'+\mu^{-1}} - \frac{x'\mu^{-1}}{4(x'+\mu^{-1})}\Phi(L_{n+1};x',\lambda_n,\mu^{-1})\right\} + \mathbf{P}^m_{\mathrm{c}}(-\mu,\mu')\omega_n\left\{-\frac{x'\sigma_{nk}}{\lambda_n^2}\frac{E_n(\mu,\lambda_n)}{x'+\mu^{-1}} + \frac{x'}{\lambda_n}\frac{F_{nk}(\mu,\lambda_n)}{x'+\mu^{-1}} - \frac{x'\mu^{-1}}{4(x'+\mu^{-1})}\Gamma^2_{nk}(x',\lambda_n,\mu^{-1})\right\}, \tag{A.9c}$$

$$\mathbf{W}^m_{4,nk}(-\mu,\mu') = \Gamma^2_{nk}(x',\lambda_n,\mu^{-1})\mathbf{R}^m_{1,\mathrm{s}}(L_n;-\mu,\mu') + \mathbf{S}^m_{4,nk}\boldsymbol{\Phi}(L_{n+1};x',\lambda_n,\mu^{-1}) + \left\{\mathbf{J}^m_{nk}(-\mu,\mu')\omega_n + \mathbf{P}^m_{\mathrm{s}}(-\mu,\mu')u_n\delta_{nk}\right\}\left\{\frac{x'}{\lambda_n}\frac{E_n(\mu,\lambda_n)}{x'+\mu^{-1}} - \frac{x'\mu^{-1}}{4(x'+\mu^{-1})}\boldsymbol{\Phi}(L_{n+1};x',\lambda_n,\mu^{-1})\right\} + \mathbf{P}^m_{\mathrm{s}}(-\mu,\mu')\omega_n\left\{-\frac{x'\sigma_{nk}}{\lambda_n^2}\frac{E_n(\mu,\lambda_n)}{x'+\mu^{-1}} + \frac{x'}{\lambda_n}\frac{F_{nk}(\mu,\lambda_n)}{x'+\mu^{-1}} - \frac{x'\mu^{-1}}{4(x'+\mu^{-1})}\boldsymbol{\Gamma}^2_{nk}(x',\lambda_n,\mu^{-1})\right\}. \tag{A.9d}$$

The sine terms can be similarly evaluated. We obtain:

$$
\begin{aligned}
L_k[\mathbf{R}^m_{2,\mathrm{s}}(L_{n+1};-\mu,\mu_0)] &= L_k[\mathbf{R}^m_{2,\mathrm{s}}(L_n;-\mu,\mu_0)]Q_n(\mu,\lambda_n) + \mathbf{R}^m_{2,\mathrm{s}}(L_n;-\mu,\mu_0)H_{nk}(\mu,\lambda_n)\\
&+\frac{1}{2\mu}\int_0^1 \mathbf{V}^m_2(-\mu',\mu_0)[\omega_n\mathbf{G}^m_{nk}(-\mu,-\mu')+u_n\delta_{nk}\mathbf{P}^m_{\mathrm{c}}(-\mu,-\mu')]\,\mathrm{d}\mu'\\
&+\frac{1}{2\mu}\int_0^1 \mathbf{W}^m_{2,nk}(-\mu',\mu_0)\omega_n\mathbf{P}^m_{\mathrm{c}}(-\mu,-\mu')\,\mathrm{d}\mu'\\
&+\frac{\lambda_n}{2}\int_0^1 \mathbf{V}_3(-\mu,\mu')[\omega_n\mathbf{J}^m_{nk}(\mu',\mu_0)+u_n\delta_{nk}\mathbf{P}^m_{s}(\mu',\mu_0)]\,\mathrm{d}\mu'\\
&+\frac{\lambda_n}{2}\int_0^1 \mathbf{W}^m_{3,nk}(-\mu,\mu')\omega_n\mathbf{P}^m_{\mathrm{s}}(\mu',\mu_0)\,\mathrm{d}\mu' + \frac{\omega_n\sigma_{nk}}{2}\int_0^1 \mathbf{V}_3(-\mu,\mu')\mathbf{P}^m_{\mathrm{s}}(\mu',\mu_0)\,\mathrm{d}\mu'\\
&-\frac{1}{2\mu}\int_0^1 \mathbf{V}_1(-\mu',\mu_0)[\omega_n\mathbf{J}^m_{nk}(-\mu,-\mu')+u_n\delta_{nk}\mathbf{P}^m_{s}(-\mu,-\mu')]\,\mathrm{d}\mu'\\
&-\frac{1}{2\mu}\int_0^1 \mathbf{W}^m_{1,nk}(-\mu',\mu_0)\omega_n\mathbf{P}^m_{\mathrm{s}}(-\mu,-\mu')\,\mathrm{d}\mu'\\
&+\frac{\lambda_n}{2}\int_0^1 \mathbf{V}_4(-\mu,\mu')[\omega_n\mathbf{G}^m_{nk}(\mu',\mu_0)+u_n\delta_{nk}\mathbf{P}^m_{\mathrm{c}}(\mu',\mu_0)]\,\mathrm{d}\mu'\\
&+\frac{\lambda_n}{2}\int_0^1 \mathbf{W}^m_{4,nk}(-\mu,\mu')\omega_n\mathbf{P}^m_{\mathrm{c}}(\mu',\mu_0)\,\mathrm{d}\mu' + \frac{\omega_n\sigma_{nk}}{2}\int_0^1 \mathbf{V}_4(-\mu,\mu')\mathbf{P}^m_{\mathrm{c}}(\mu',\mu_0)\,\mathrm{d}\mu'.
\end{aligned}
\tag{A.10}
$$

This completes the linearization for the vector reflection matrices. Now we consider the cosine-only contribution required for the intensity correction. Defining:

$$S^m_{1,nk} \equiv L_k[R^m_{1,\mathrm{c}}(L_{n+1};-\mu',\mu_0)], \tag{A.11a}$$

$$S^m_{3,nk} \equiv L_k[R^m_{1,\mathrm{c}}(L_{n+1};-\mu,\mu')], \tag{A.11b}$$

$$W^m_{1,nk} \equiv L_k[V_1], \tag{A.11c}$$

$$W^m_{3,nk} \equiv L_k[V_3], \tag{A.11d}$$

we get the relations:

$$
\begin{aligned}
S^m_{1,nk} &= L_k[R^m_{1,\mathrm{c}}(L_n;-\mu',\mu_0)]Q_n(\mu',\lambda_n) + R^m_{1,\mathrm{c}}(L_n;-\mu',\mu_0)H_{nk}(\mu',\lambda_n)\\
&+\omega_n E_n(\mu',\lambda_n)G^m_{nk}(-\mu',\mu_0) + P^m_{\mathrm{c}}(-\mu',\mu_0)[F_{nk}(\mu',\lambda_n)\omega_n + E_n(\mu',\lambda_n)u_n\delta_{nk}],
\end{aligned}
\tag{A.12a}
$$

$$
\begin{aligned}
S^m_{3,nk} &= L_k[R^m_{1,\mathrm{c}}(L_n;-\mu,\mu')]Q_n(\mu,x') + R^m_{1,\mathrm{c}}(L_n;-\mu,\mu')]H_{nk}(\mu,x')\\
&+\omega_n E_n(\mu,x')G^m_{nk}(-\mu,\mu') + P^m_{\mathrm{c}}(-\mu,\mu')[F_{nk}(\mu,x')\omega_n + E_n(\mu,x')u_n\delta_{nk}],
\end{aligned}
\tag{A.12b}
$$

$$
\begin{aligned}
W^m_{1,nk}(-\mu',\mu_0) &= \Gamma^1_{nk}(\mu^{-1},x',\lambda_n)R^m_{1,\mathrm{c}}(L_n;-\mu',\mu_0) + S^m_{1,nk}\Phi(L_{n+1};\mu^{-1},x',\lambda_n)\\
&+\left\{G^m_{nk}(-\mu',\mu_0)\omega_n + P^m_{\mathrm{c}}(-\mu',\mu_0)u_n\delta_{nk}\right\}\left\{\frac{x'}{\mu^{-1}}\frac{E_n(\mu,\lambda_n)}{x'+\lambda_n} - \frac{x'\lambda_n}{4(x'+\lambda_n)}\Phi(L_{n+1};\mu^{-1},x',\lambda_n)\right\}\\
&+P^m_{\mathrm{c}}(-\mu',\mu_0)\omega_n\left\{\begin{array}{l}\frac{x'}{\mu^{-1}}\frac{F_{nk}(\mu,\lambda_n)}{x'+\lambda_n} - \frac{x'}{\mu^{-1}}\frac{E_n(\mu,\lambda_n)\sigma_{nk}}{(x'+\lambda_n)^2} - \frac{x'\sigma_{nk}}{4(x'+\lambda_n)}\Phi(L_{n+1};\mu^{-1},x',\lambda_n)\\ +\frac{x'\lambda_n\sigma_{nk}}{4(x'+\lambda_n)^2}\Phi(L_{n+1};\mu^{-1},x',\lambda_n) - \frac{x'\lambda_n}{4(x'+\lambda_n)}\Gamma^1_{nk}(\mu^{-1},x',\lambda_n)\end{array}\right\},
\end{aligned}
\tag{A.12c}
$$

$$W^m_{3,nk}(-\mu,\mu') = \Gamma^2_{nk}(x',\lambda_n,\mu^{-1})R^m_{1,c}(L_n;-\mu,\mu') + S^m_{3,nk}\Phi(L_{n+1};x',\lambda_n,\mu^{-1})$$
$$+ \left\{G^m_{nk}(-\mu,\mu')\omega_n + P^m_c(-\mu,\mu')u_n\delta_{nk}\right\}\left\{\frac{x'}{\lambda_n}\frac{E_n(\mu,\lambda_n)}{x'+\mu^{-1}} - \frac{x'\mu^{-1}}{4(x'+\mu^{-1})}\Phi(L_{n+1};x',\lambda_n,\mu^{-1})\right\}$$
$$+ P^m_c(-\mu,\mu')\omega_n\left\{-\frac{x'\sigma_{nk}}{\lambda_n^2}\frac{E_n(\mu,\lambda_n)}{x'+\mu^{-1}} + \frac{x'}{\lambda_n}\frac{F_{nk}(\mu,\lambda_n)}{x'+\mu^{-1}} - \frac{x'\mu^{-1}}{4(x'+\mu^{-1})}\Gamma^2_{nk}(x',\lambda_n,\mu^{-1})\right\}, \tag{A.12d}$$

where G^m_{nk} is the (1,1) element of $\mathbf{G}^m_{nk}$.

We also obtain the following relation for the Fourier component, $R^m_{2,c}$, of the scalar reflection function:

$$L_k[R^m_{2,c}(L_{n+1};-\mu,\mu_0)] = L_k[R^m_{2,c}(L_n;-\mu,\mu_0)]Q_n(\mu,\lambda_n) + R^m_{2,c}(L_n;-\mu,\mu_0)H_{nk}(\mu,\lambda_n)$$
$$+\frac{1}{2\mu}\int_0^1 V^m_1(-\mu',\mu_0)[\omega_n G^m_{nk}(-\mu,-\mu') + u_n\delta_{nk}P^m_c(-\mu,-\mu')]\,d\mu'$$
$$+\frac{1}{2\mu}\int_0^1 W^m_{1,nk}(-\mu',\mu_0)\omega_n P^m_c(-\mu,-\mu')\,d\mu' + \frac{\lambda_n}{2}\int_0^1 V^m_3(-\mu,\mu')[\omega_n G^m_{nk}(\mu',\mu_0) + u_n\delta_{nk}P^m_c(\mu',\mu_0)]\,d\mu'$$
$$+\frac{\lambda_n}{2}\int_0^1 W^m_{3,nk}(-\mu,\mu')\omega_n P^m_c(\mu',\mu_0)\,d\mu' + \frac{\omega_n\sigma_{nk}}{2}\int_0^1 V^m_3(-\mu,\mu')P^m_c(\mu',\mu_0)\,d\mu'. \tag{A.13}$$

Finally, Eqs. (32), (A.3) and (A.13) can be used to calculate the linearization of the Fourier components of the intensity correction at the TOA:

$$L_k[I^m_{corr}(\tau_{N+1})] = L_k[\mathbf{R}^m_{2,c}(\tau_{N+1};-\mu,\mu_0)]|_{(1,1)} - L_k[R^m_2(\tau_{N+1};-\mu,\mu_0)]. \tag{A.14}$$

References

[1] Hansen JE, Travis LD. Light scattering in planetary atmospheres. Space Sci Rev 1974;16:527–610.
[2] Schulz FM, Stamnes K, Weng F. VDISORT: an improved and generalized discrete ordinate method for polarized (vector) radiative transfer. JQSRT 1999;61(1):105–22.
[3] Spurr RJD. VLIDORT: a linearized pseudo-spherical vector discrete ordinate radiative transfer code for forward model and retrieval studies in multilayer multiple scattering media. JQSRT 2006;102(2):316–42.
[4] de Haan JF, Bosma PB, Hovenier JW. The adding method for multiple scattering calculations of polarized light. Astron Astrophys 1987;183(2):371–91.
[5] Mishchenko MI. The fast invariant imbedding method for polarized light: computational aspects and numerical results for Rayleigh scattering. JQSRT 1990;43(2):163–71.
[6] Hovenier JW. Multiple scattering of polarized light in planetary atmospheres. Astron Astrophys 1971;13:7–29.
[7] Kawabata K, Ueno S. The first three orders of scattering in vertically inhomogeneous scattering–absorbing media. Astrophys Space Sci 1988;150:327–44.
[8] Spurr RJD. Simultaneous derivation of intensities and weighting functions in a general pseudo-spherical discrete ordinate radiative transfer treatment. JQSRT 2002;75(2):129–75.
[9] Rodgers CD. Inverse methods for atmospheric sounding: theory and practice. Singapore: World Scientific; 2000.
[10] Natraj V, Bösch H, Spurr RJD, Yung YL. Improving trace gas retrievals from near infrared satellite measurements by fast and accurate vector radiative transfer modeling. J Geophys Res [manuscript in preparation].
[11] Thomas GE, Stamnes K. Radiative transfer in the atmosphere and ocean. New York: Cambridge University Press; 1999.
[12] Mishchenko MI, Hovenier JW, Travis LD, editors. Light scattering by nonspherical particles: theory, measurements and applications. San Diego: Academic Press; 2000.
[13] Siewert CE. On the phase matrix basic to the scattering of polarized light. Astron Astrophys 1982;109:195–200.
[14] Dahlback A, Stamnes K. A new spherical model for computing the radiation field available for photolysis and heating at twilight. Planet Space Sci 1991;39:671–83.
[15] Caudill TR, Flittner DE, Herman BM, Torres O, McPeters RD. Evaluation of the pseudo-spherical approximation for backscattered ultraviolet radiances and ozone retrieval. J Geophys Res 1997;102:3881–90.
[16] Mishchenko MI, Travis LD. Satellite retrieval of aerosol properties over the ocean using polarization as well as intensity of reflected sunlight. J Geophys Res 1997;102(D14):16989–7013.
[17] Cox C, Munk W. Statistics of the sea surface derived from sun glitter. J Mar Res 1954;13:198–227.
[18] Tsang L, Kong JA, Shin RT. Theory of microwave remote sensing. New York: Wiley; 1985.
[19] O'Brien DM, English SA, da Costa GA. High-precision, high-resolution measurements of absorption in the oxygen *A*-band. J Atmos Ocean Tech 1997;14(1):105–19.

[20] O'Brien DM, Mitchell RM, English SA, da Costa GA. Airborne measurements of air mass from O_2 *A*-band absorption spectra. J Atmos Ocean Tech 1998;15(6):1272–86.
[21] O'Brien DM, Mitchell RM. Error estimates for retrieval of cloud-top pressure using absorption in the *A* band of oxygen. J Appl Meteorol 1992;31(10):1179–92.
[22] Kuze A, Chance KV. Analysis of cloud top height and cloud coverage from satellite using the O_2 A and B bands. J Geophys Res 1994;99(D7):14481–92.
[23] Koelemeijer RBA, Stammes P, Hovenier JW, de Haan JF. A fast method for retrieval of cloud parameters using oxygen A band measurements from the Global Ozone Monitoring Experiment. J Geophys Res 2001;106(D4):3475–90.
[24] Rozanov VV, Kokhanovsky AA. Semianalytical cloud retrieval algorithm as applied to the cloud top altitude and the cloud geometrical thickness determination from top-of-atmosphere reflectance measurements in the oxygen *A* band. J Geophys Res 2004;109(D5):D05202.
[25] Rozanov VV, Kokhanovsky AA, Burrows JP. The determination of cloud altitudes using GOME reflectance spectra: multilayered cloud systems. IEEE Trans Geosci Remote Sens 2004;42(5):1009–17.
[26] US standard atmosphere. Washington, DC: US Government Printing Office; 1976.
[27] Rothman LS, Jacquemart D, Barbe A, Benner DC, Birk M, Brown LR, et al. The HITRAN 2004 molecular spectroscopic database. JQSRT 2005;96(2):139–204.
[28] van de Hulst HC. Light scattering by small particles. New York: Wiley; 1957.
[29] Young AT. Revised depolarization corrections for atmospheric extinction. Appl Opt 1980;19(20):3427–8.
[30] Kahn R, Banerjee P, McDonald D. Sensitivity of multiangle imaging to natural mixtures of aerosols over ocean. J Geophys Res 2001;106(D16):18219–38.
[31] 〈http://www.eumetcal.org/eurometcal/english/satmet/s2400/s240009d.htm〉.
[32] Palmer KF, Williams D. Optical constants of sulfuric acid; application to the clouds of Venus? Appl Opt 1975;14(1):208–19.
[33] de Rooij WA, van der Stap CCAH. Expansion of Mie scattering matrices in generalized spherical functions. Astron Astrophys 1984;131(2):237–48.
[34] Mishchenko MI, Travis LD. Capabilities and limitations of a current Fortran implementation of the *T*-matrix method for randomly oriented, rotationally symmetric scatterers. JQSRT 1998;60(3):309–24.